© 2022. Published by The Company of Biologists Ltd | Development (2022) 149, dev200536. doi:10.1242/dev.200536

RESEARCH ARTICLE

AMPK activates the Nrf2-Keap1 pathway to govern dendrite pruning via the insulin pathway in *Drosophila*

Liang Yuh Chew[1,2], Jianzheng He[1], Jack Jing Lin Wong[1], Sheng Li[3] and Fengwei Yu[1,2,*]

ABSTRACT

During *Drosophila* metamorphosis, the ddaC dendritic arborisation sensory neurons selectively prune their larval dendrites in response to steroid hormone ecdysone signalling. The Nrf2-Keap1 pathway acts downstream of ecdysone signalling to promote proteasomal degradation and thereby dendrite pruning. However, how the Nrf2-Keap1 pathway is activated remains largely unclear. Here, we demonstrate that the metabolic regulator AMP-activated protein kinase (AMPK) plays a cell-autonomous role in dendrite pruning. Importantly, AMPK is required for Mical and Headcase expression and for activation of the Nrf2-Keap1 pathway. We reveal that AMPK promotes the Nrf2-Keap1 pathway and dendrite pruning partly via inhibition of the insulin pathway. Moreover, the AMPK-insulin pathway is required for ecdysone signalling to activate the Nrf2-Keap1 pathway during dendrite pruning. Overall, this study reveals an important mechanism whereby ecdysone signalling activates the Nrf2-Keap1 pathway via the AMPK-insulin pathway to promote dendrite pruning, and further suggests that during the nonfeeding prepupal stage metabolic alterations lead to activation of the Nrf2-Keap1 pathway and dendrite pruning.

KEY WORDS: AMPK kinase, Dendrite pruning, Ecdysone signalling, Insulin pathway, Metamorphosis, Nrf2-Keap1 pathway

INTRODUCTION

During animal development, neurons often form exuberant or incorrect axons and dendrites at early stages, followed by the refinement of neuronal circuits at later stages. Pruning, a developmental process that specifically removes unwanted neurites without loss of neurons, is crucial for refinement of the nervous systems (Luo and O'Leary, 2005; Riccomagno and Kolodkin, 2015; Schuldiner and Yaron, 2015). Impaired pruning, which results in altered synaptic density in human brains, is often associated with autism-spectrum disorders (Tang et al., 2014) or schizophrenia (Sellgren et al., 2019). Thus, understanding the mechanisms of neuronal pruning would provide some important insights into the pathogenesis of human brain disorders. In the holometabolous insect *Drosophila*, dendritic arborisation (da) sensory neurons and mushroom body γ neurons have been utilised as two major models to elucidate the molecular and cellular mechanisms of neuronal pruning during metamorphosis (Yu and Schuldiner, 2014). A subset of dorsal da neurons, including ddaC (also known as C4da) and ddaD/E neurons, prune away all the larval dendrites but keep their axons intact (Kuo et al., 2005; Shimono et al., 2009; Williams and Truman, 2005), whereas mushroom body γ neurons prune their dendrites as well as some of axonal branches (Lee et al., 2000; Schuldiner and Yaron, 2015). In ddaC neurons, the proximal regions of dendrites undergo blebbing, thinning and subsequent severing around 6 h after puparium formation (APF), followed by dendrite fragmentation and clearance by 16 h APF (Fig. 1A) (Kuo et al., 2005; Williams and Truman, 2005).

In *Drosophila*, neuronal pruning is triggered by a pulse of the steroid hormone ecdysone secreted at the late larval stage (Consoulas et al., 2000; Truman, 1990). Ecdysone binds to the ecdysone receptor complex comprising the ecdysone receptor (EcR) and Ultraspiracle (Usp), and thereby activates the transcription of its downstream response genes (Thummel, 1996). In ddaC or mushroom body γ neurons, the neuronal isoform EcR-B1 is upregulated at the wandering third instar larval (wL3) and white prepupal (WP) stages (Kirilly et al., 2009; Kuo et al., 2005; Lee et al., 2000). EcR-B1 expression depends on TGFβ signalling (Wong et al., 2013; Zheng et al., 2003), the cohesin complex (Schuldiner et al., 2008), the nuclear receptors Ftz-F1 and Hr39 (Boulanger et al., 2011) and the BTB-zinc finger transcription factor Chinmo (Alyagor et al., 2018; Marchetti and Tavosanis, 2017). In ddaC neurons, the target genes of ecdysone signalling are temporally induced by coordinated action between EcR-B1 and two chromatin remodellers [Brahma and CREB-binding protein (Nej)] (Kirilly et al., 2011). EcR-B1 and Usp induce the expression of the key transcription factor Sox14 and a cytosolic protein Headcase (Hdc) of unknown function (Kirilly et al., 2009; Loncle and Williams, 2012). Sox14 in turn promotes the expression of its target genes, including the F-actin disassembly factor Mical and components of the ubiquitin-proteasome degradation pathway (Kirilly et al., 2011; Rode et al., 2018; Rumpf et al., 2011; Wong et al., 2013). Recently, we reported that the Nrf2-Keap1 pathway is activated by ecdysone signalling to promote dendrite pruning in ddaC neurons (Chew et al., 2021). CncC, the sole fly homologue of Nrf2, is upregulated by EcR-B1 and Sox14 before the onset of dendrite pruning. Interestingly, the Nrf2-Keap1 pathway regulates dendrite pruning through the proteasomal degradation pathway, rather than the canonical antioxidant response pathway (Chew et al., 2021). However, how ecdysone signalling activates the Nrf2-Keap1 pathway in dendrite pruning remained elusive; moreover, whether and how metabolic regulators or pathways are required for the activation of the Nrf2-Keap1 pathway during the larval-pupal transition were largely unknown.

In an RNA-interference (RNAi) screen, we identified that AMPKα, a catalytic subunit of the trimeric adenosine monophosphate activated protein kinase (AMPK), plays an important role in dendrite pruning. AMPK, which consists of three

[1]Temasek Life Sciences Laboratory, 1 Research Link, National University of Singapore, 117604, Singapore. [2]Department of Biological Sciences, National University of Singapore, 117543, Singapore. [3]Guangdong Provincial Key Laboratory of Insect Developmental Biology and Applied Technology, Institute of Insect Science and Technology & School of Life Sciences, South China Normal University, Guangzhou 510631, China.

*Author for correspondence (fengwei@tll.org.sg)

L.Y., 0000-0002-0397-3698; J.J.L.W., 0000-0002-9547-4692; F.Y., 0000-0003-0268-199X

Handling Editor: François Guillemot
Received 18 January 2022; Accepted 16 June 2022

Development (2022) 149, dev200536. doi:10.1242/dev.200536

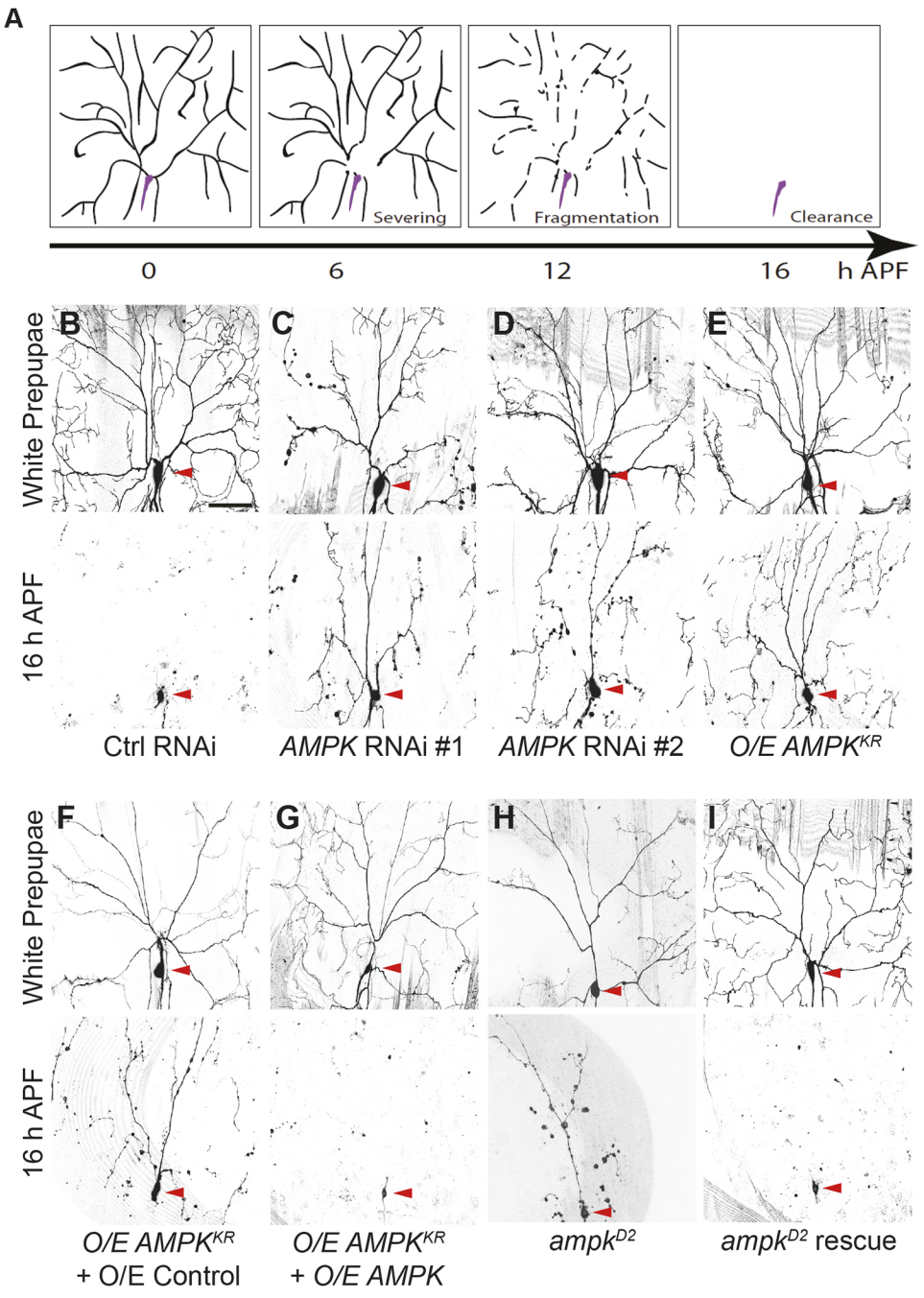

Fig. 1. AMPK is cell-autonomously required for dendrite pruning in ddaC neurons. (A) Schematic of the dendrite pruning process in ddaC sensory neurons. Soma and axon are shown in purple. (B-I) Dendrites of control (Ctrl) (B), *AMPK* RNAi #1 (C), *AMPK* RNAi #2 (D), $AMPK^{KR}$ (E), $AMPK^{KR}$+overexpressing (O/E) control (F), $AMPK^{KR}$+*O/E AMPK* (G), $ampk^{D2}$ (H) and $ampk^{D2}$ rescue (I) ddaC neurons at WP and 16 h APF stages. Red arrowheads point to the somata of ddaC neurons. (J) Percentages of ddaC neurons showing the dendrite pruning defects at 16 h APF. (K) Quantitative analysis of unpruned dendrite length at 16 h APF. Error bars represent s.e.m. Two-tailed Student's *t*-test was used to determine statistical significance for pairwise comparison, whereas one-way ANOVA with Bonferroni test was applied to determine significance for multiple-group comparison. ns, not significant; ****P<0.0001. The number of neurons (n) examined in each group is shown on the bars. Scale bar: 50 μm.

Development (2022) 149, dev200536. doi:10.1242/dev.200536

subunits (AMPKα, AMPKβ and AMPKγ), is an important metabolic regulator that controls energy homeostasis at cellular and organismal levels. AMPK can be activated in response to high cellular AMP/ATP or ADP/ATP ratio upon energy deprivation. Activated AMPK maintains energy homeostasis by promoting catabolism and suppressing anabolism (Hardie et al., 2012; Trefts and Shaw, 2021). In *Drosophila*, AMPK has been reported to regulate cell polarity, morphogenesis, autophagy, ageing and neurodegenerative diseases (Lee et al., 2007; Ng et al., 2012; Swick et al., 2013; Ulgherait et al., 2014). In fly and silkworm fat bodies, both AMPK expression and activity are activated by ecdysone signalling during larval moulting or pupariation. Upon activation, AMPK activates Protein phosphatase 2A (PP2A) to antagonise insulin pathway and restrict growth rate (Yuan et al., 2020). Despite the important role of AMPK in regulating metabolism and growth, its potential functions in neuronal pruning remained unknown. Moreover, our previous studies also indicate that ecdysone signalling promotes dendrite pruning of ddaC neurons by inhibiting the insulin pathway and activating the Nrf2-Keap1 pathway during the larval-pupal transition (Chew et al., 2021; Wong et al., 2013), raising the possibility that the Nrf2-Keap1 pathway might be activated in response to metabolic changes during the nonfeeding prepupal stage. Here, we report a cell-autonomous role of the metabolic regulator AMPK in dendrite pruning of ddaC neurons. Our genetic study demonstrates a pathway in which AMPK is required to activate the Nrf2-Keap1 pathway and promote dendrite pruning via attenuation of the insulin pathway. We show that the AMPK-insulin pathway is required for ecdysone signalling to activate the Nrf2-Keap1 pathway during dendrite pruning. Thus, this study suggests that during early metamorphosis hormonal and metabolic changes lead to activation of the Nrf2-Keap1 pathway, which in turn facilitates dendrite pruning.

RESULTS

AMPK is cell-autonomously required for dendrite pruning of ddaC neurons

To study the mechanisms of dendrite pruning in ddaC sensory neurons systematically, we previously conducted a large-scale RNAi screen using the class IV da-specific driver *pickpocket* (*ppk*)-*Gal4* to express various transgenic RNAi lines (Kirilly et al., 2009, 2011). From this screen, we isolated two independent lines for the catalytic subunit of AMPK (AMPKα, called AMPK hereafter), namely v106200 (#1) and BL25931 (#2). Knockdown of AMPK using either of these RNAi lines led to consistent dendrite pruning defects, including both severing and fragmentation defects, in ddaC neurons at 16 h APF (#1, 77%; #2, 54%) (Fig. 1C,D,J, Fig. S1A). In contrast, wild-type ddaC neurons, which were derived from the control RNAi line v25271 targeting the germ cell-specific gene *γ-Tub37C*, pruned away all their larval dendrites at the same time point (Fig. 1B,J,K). AMPK is evolutionarily conserved from yeast to humans, and functions as a metabolic or energy sensor that is activated upon energy deprivation. We further verified the function of AMPK in dendrite pruning using the kinase-dead form of AMPK ($AMPK^{KR}$) and the *ampk* mutant. Overexpression of $AMPK^{KR}$ caused similar dendrite pruning defects in 67% of ddaC neurons (Fig. 1E,J,K). The $AMPK^{KR}$ defects were fully rescued by expression of wild-type AMPK (Fig. 1G,J,K), but not by expression of the non-functional N-terminal Mical ($Mical^{NT}$) control (Fig. 1F,J,K) (Kirilly et al., 2009). The rescue data attests to the specific effect of $AMPK^{KR}$. Moreover, we also generated mosaic analysis with a repressible cell marker (MARCM) mutant ddaC clones using the *ampk* null allele $ampk^{D2}$ (Lee et al., 2007), which exhibited consistent dendrite pruning defects at 16 h APF (Fig. 1H,J,K), compared with the control clones (Fig. 1J,K). The $ampk^{D2}$-associated pruning defects were fully rescued by the expression of AMPK (Fig. 1I-K). These data highlight a cell-autonomous role of AMPK in dendrite pruning of ddaC neurons. To assess whether AMPK activation can accelerate dendrite pruning, we overexpressed either wild-type AMPK or $AMPK^{TD}$, a constitutively active form of AMPK ($AMPK^{CA}$), in ddaC neurons. Overexpression of AMPK or $AMPK^{CA}$ neither promoted precocious dendrite pruning at 6 h APF nor inhibited dendrite pruning at 16 h APF (Fig. S1B). Taken together, our data indicate that the metabolic regulator AMPK is required but not sufficient to promote dendrite pruning in ddaC sensory neurons.

AMPK is required for the expression of Mical and Hdc

Previous studies by ourselves and others have demonstrated that ddaC dendrite pruning requires ecdysone signalling as well as its downstream pathways including the proteasomal degradation pathway, the insulin pathway, the Nrf2-Keap1 pathway and microtubule orientation/disassembly (Bu et al., 2021; Chew et al., 2021; Herzmann et al., 2018; Kuo et al., 2005, 2006; Tang et al., 2020; Wang et al., 2019; Williams and Truman, 2005; Wong et al., 2013). We therefore systematically investigated the potential involvement of AMPK in these known pathways. We first assessed whether AMPK is required for activation of ecdysone signalling during dendrite pruning. Protein levels of EcR-B1, Sox14, Hdc and Mical are upregulated in ddaC neurons at the WP stage when ecdysone signalling is activated (Kirilly et al., 2009; Kuo et al., 2005; Loncle and Williams, 2012). Interestingly, compared with those in wild-type neurons (Fig. S2A,B), upregulation of EcR-B1 and Sox14 protein levels was not altered in AMPK RNAi or $AMPK^{KR}$-expressing ddaC neurons at the WP stage (Fig. S2A,B), in contrast with a recent study showing that AMPK regulates general gene translation in ddaC neurons (Marzano et al., 2021). In contrast, upregulation of Mical and Hdc expression was impaired at the WP stage, as their protein levels were significantly reduced in AMPK RNAi or $AMPK^{KR}$-expressing ddaC neurons (Fig. S2C,D). The reduced Mical and Hdc levels could be due to impaired translation rate in AMPK RNAi neurons (Marzano et al., 2021). Mical is an F-actin-disassembly factor that regulates cytoskeletal disassembly in axonal growth and bristle elongation (Hung et al., 2010). However, whether Mical regulates F-actin disassembly during dendrite pruning remains unknown. Hdc is upregulated during dendrite pruning, and its exact function during dendrite pruning remains to be determined (Loncle and Williams, 2012). Whereas Mical upregulation depends on both EcR and Sox14 (Kirilly et al., 2009), Hdc expression is regulated by EcR but not by Sox14 (Loncle and Williams, 2012). Our data suggest that AMPK might modulate the expression of various pruning factors downstream of both EcR and Sox14. Thus, AMPK is required for Mical and Hdc expression but dispensable for EcR and Sox14 upregulation during dendrite pruning.

To investigate how AMPK regulates Mical expression, we generated a *Mical1-lacZ* reporter that drives the upregulation of β-galactosidase (encoded by *lacZ*) expression in ddaC neurons under the control of a *Mical* enhancer. From the regulatory region upstream of the *Mical* start codon, four genomic fragments (*mical1-4*) were amplified and inserted upstream of the *lacZ* coding sequence (Fig. S3A). Among them, the *mical1-lacZ* transgene fully resembled the temporal expression of *Mical* in ddaC neurons (Kirilly et al., 2009). β-Galactosidase expression was absent in ddaC neurons at the early third instar larval (eL3) and wL3 stages but was strongly upregulated at the WP stage (Fig. S3B). The β-galactosidase expression coincided with upregulation of Mical expression at the WP stage (Fig. S3C). Moreover, β-galactosidase

Development (2022) 149, dev200536. doi:10.1242/dev.200536

upregulation was largely abolished upon knockdown of EcR or Sox14 (Fig. S3D). Therefore, *mical1-lacZ* is a reliable reporter that reflects the temporal expression of *Mical* in ddaC neurons. Importantly, *mical1-lacZ* expression was almost lost at the WP stage in AMPK RNAi or AMPK^{KR}-expressing ddaC neurons (Fig. S3E). These *mical1-lacZ* data suggest that AMPK is required to activate Mical expression, likely via transcriptional regulation. It complements a recent study suggesting that AMPK might regulate Mical translation during dendrite pruning (Marzano et al., 2021). In summary, AMPK is required for ecdysone signalling to induce the expression of Mical and Hdc during dendrite pruning.

Rpn7, a regulatory subunit of the 26S proteasome, is a downstream target of the Nrf2-Keap1 pathway during dendrite pruning

Our recent study reported that ecdysone signalling activates the Nrf2-Keap1 pathway to promote dendrite pruning; moreover, the Nrf2-Keap1 pathway upregulates proteasome gene transcription and proteasomal degradation activity prior to dendrite pruning (Chew et al., 2021). We next assessed whether AMPK is required for the activation of the Nrf2-Keap1 pathway, in addition to ecdysone signalling. To improve detection of activation of the Nrf2-Keap1 pathway in ddaC neurons, we first isolated potential proteasomal subunits for which expression depends on the Nrf2-Keap1 pathway. Using available antibodies against fly proteasomal subunits, we isolated Rpn7 as a downstream target of the Nrf2-Keap1 pathway and used it as a reporter of the pathway to study the epistasis between AMPK and the Nrf2-Keap1 pathway. The anti-Rpn7 antibody staining assays indicated that Rpn7 was weakly expressed in the cytoplasm of ddaC neurons at wL3 and WP stages (Fig. 2A, Fig. S4C), but was significantly upregulated with enrichment in the nuclei at 6 and 8 h APF (Fig. 2A). The anti-Rpn7 antibody is specific, as the signals were strongly reduced in ddaC neurons expressing either of two independent *Rpn7* RNAi constructs (#1, BL#34787; #2, v101467) (Fig. S4A). Knockdown of Rpn7 by either of these RNAi lines led to consistent dendrite pruning defects (Fig. S4B), confirming the importance of the proteasomal degradation machinery during dendrite pruning (Kuo et al., 2005). Importantly, RNAi knockdown of CncC (the fly homologue of Nrf2) by two RNAi lines (#1 and #2) significantly reduced Rpn7 expression at 6 h APF (Fig. 2B). Conversely, when CncC was overexpressed in ddaC neurons, Rpn7 expression was significantly elevated from wL3 to 6 h APF (Fig. 2D, Fig. S4C). Moreover, ecdysone signalling is responsible for upregulation of Rpn7 expression, as RNAi knockdown of EcR or Sox14 led to a significant reduction in Rpn7 protein levels at 6 h APF (Fig. 2C). However, the F-actin disassembly regulator Mical is not required for Rpn7 upregulation at 6 h APF (Fig. S4A). Overexpression of Sox14, which has been shown to precociously activate ecdysone signalling (Kirilly et al., 2009), caused significant increases in Rpn7 levels in ddaC neurons at 3 and 6 h APF (Fig. 2D, Fig. S4C). Taken together, we conclude that the regulatory subunit of the 26S proteasome Rpn7 is a downstream target of the Nrf2-Keap1 pathway, which is induced by ecdysone signalling before the onset of dendrite pruning. We then utilised Rpn7 as a reporter to detect activation of the Nrf2-Keap1 pathway and proteasomal degradation pathway in the following studies.

AMPK is required for activation of the Nrf2-Keap1 pathway prior to dendrite pruning

Given that the Nrf2-Keap1 pathway can activate both the antioxidant response pathway and the proteasomal degradation pathway during dendrite pruning (Chew et al., 2021), we took advantage of two reporters, namely *gstD1-lacZ* (reflecting the antioxidant response pathway) (Hochmuth et al., 2011; Sykiotis and Bohmann, 2008) and Rpn7 (reflecting the proteasomal degradation pathway), to detect activation of the Nrf2-Keap1 pathway in ddaC neurons. When AMPK was knocked down by either of its RNAi lines, *gstD1-lacZ* expression was significantly reduced in ddaC neurons at 6 h APF (Fig. 3A). Likewise, Rpn7 expression also depends on AMPK, as its levels were significantly downregulated at 6 h APF upon AMPK RNAi knockdown (Fig. 3B). Concomitant with Rpn7 reduction, ubiquitylated proteins were robustly aggregated in numerous puncta in those AMPK RNAi ddaC neurons (Fig. 3C). However, CncC protein levels were not reduced but rather were significantly increased in AMPK RNAi or AMPK^{KR}-expressing ddaC neurons at 6 h APF (Fig. S5A). These data indicate that AMPK is unlikely to promote CncC translation, in contrast to a recent finding showing that AMPK enhances general gene translation (Marzano et al., 2021). Thus, our data from two reporters demonstrate an essential role of AMPK in activation of the Nrf2-Keap1 pathway prior to dendrite pruning. To examine whether AMPK is sufficient to activate the Nrf2-Keap1 pathway, we overexpressed either the wild-type form of AMPK or the constitutively active form (AMPK^{CA}) in ddaC neurons. Overexpression of AMPK or AMPK^{CA} did not affect the expression levels of *gstD1-lacZ* or Rpn7 at 6 h APF (Fig. 3D,E). In addition, AMPK has been reported to regulate microtubule polymerisation (Nakano et al., 2010; Yashirogi et al., 2021). However, AMPK appears to be dispensable for microtubule mass, orientation and polymerisation in the main dendrites of ddaC neurons, as the levels of the microtubule-associated protein Futsch and the movement of EB1-GFP comets were not affected in the dendrites of AMPK RNAi or AMPK^{KR}-overexpressing neurons (Fig. S5B,C). Thus, AMPK is required but not sufficient to activate the Nrf2-Keap1 pathway prior to dendrite pruning.

AMPK regulates dendrite pruning partly by activating the Nrf2-Keap1 pathway

We next investigated whether AMPK regulates dendrite pruning by activating Nrf2-Keap1 pathway. To this end, we examined whether overexpression of CncC can suppress the AMPK RNAi phenotypes. When CncC was overexpressed in AMPK RNAi (#1 or #2) ddaC neurons, the expression levels of *gstD1-lacZ* were significantly elevated at 6 h APF (Fig. 4A), compared with those in the control neurons (Fig. 4A). Overexpression of CncC was also able to significantly upregulate the expression levels of Rpn7 in ddaC neurons expressing either of the two AMPK RNAi lines (Fig. 4B), suggesting that the proteasomal degradation machinery is restored upon CncC overexpression. In line with this, the aggregation of ubiquitylated proteins was significantly reduced in AMPK RNAi neurons overexpressing CncC (Fig. 4C), in contrast to many ubiquitylated protein aggregates in AMPK RNAi control neurons (Fig. 4C). This rescue effect was specific, as ubiquitylated protein aggregates were still observed in *Rab5*^{DN} neurons overexpressing CncC, similar to those in *Rab5*^{DN} control neurons (Fig. S6A) (Zhang et al., 2014). These data suggest that CncC specifically regulates proteasomal protein degradation but not endo-lysosomal protein degradation. Moreover, double knockdown of AMPK and CncC showed a similar extent of ubiquitylated protein aggregates (Fig. S6B), compared with CncC single knockdown (Fig. S6B). These data are consistent with the conclusion that AMPK and CncC acts in the same pathway to control proteasomal degradation. More importantly, overexpression of CncC was also able to significantly suppress the dendrite pruning defects in AMPK RNAi neurons (#1

Development (2022) 149, dev200536. doi:10.1242/dev.200536

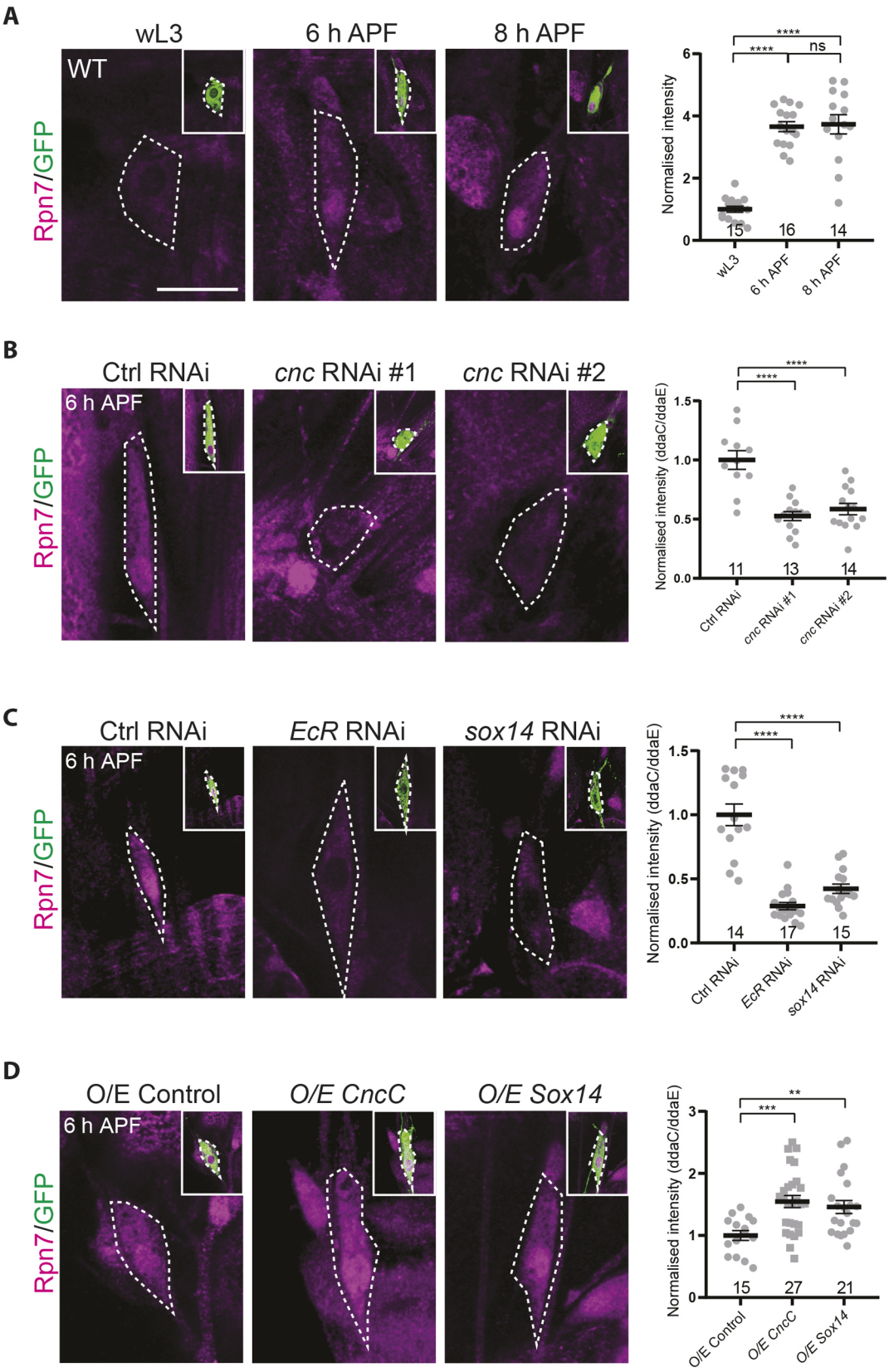

Fig. 2. Rpn7, a regulatory subunit of the 26S proteasome, is a downstream target of the Nrf2-Keap1 pathway during dendrite pruning. (A) Expression of Rpn7 in wild-type ddaC neurons at wL3, 6 h APF and 8 h APF stages. (B-D) Expression of Rpn7 in control RNAi, *Cnc* RNAi #1 and *Cnc* RNAi #2 (B); control RNAi, *EcR* RNAi and *Sox14* RNAi (C); and control, CncC-overexpressing and Sox14-overexpressing (D) ddaC neurons at 6 h APF. ddaC somata are marked by dashed lines. Insets show green fluorescent protein (GFP)-labelled ddaC neurons. Quantitative analyses of normalised Rpn7 fluorescence are shown on the right. Error bars represent s.e.m. One-way ANOVA with Bonferroni test was applied to determine significance for multiple-group comparison. ns, not significant; ***P*<0.01, ****P*<0.001, *****P*<0.0001. The number of neurons (*n*) examined in each group is shown on the bars. Scale bar: 10 µm.

Development (2022) 149, dev200536. doi:10.1242/dev.200536

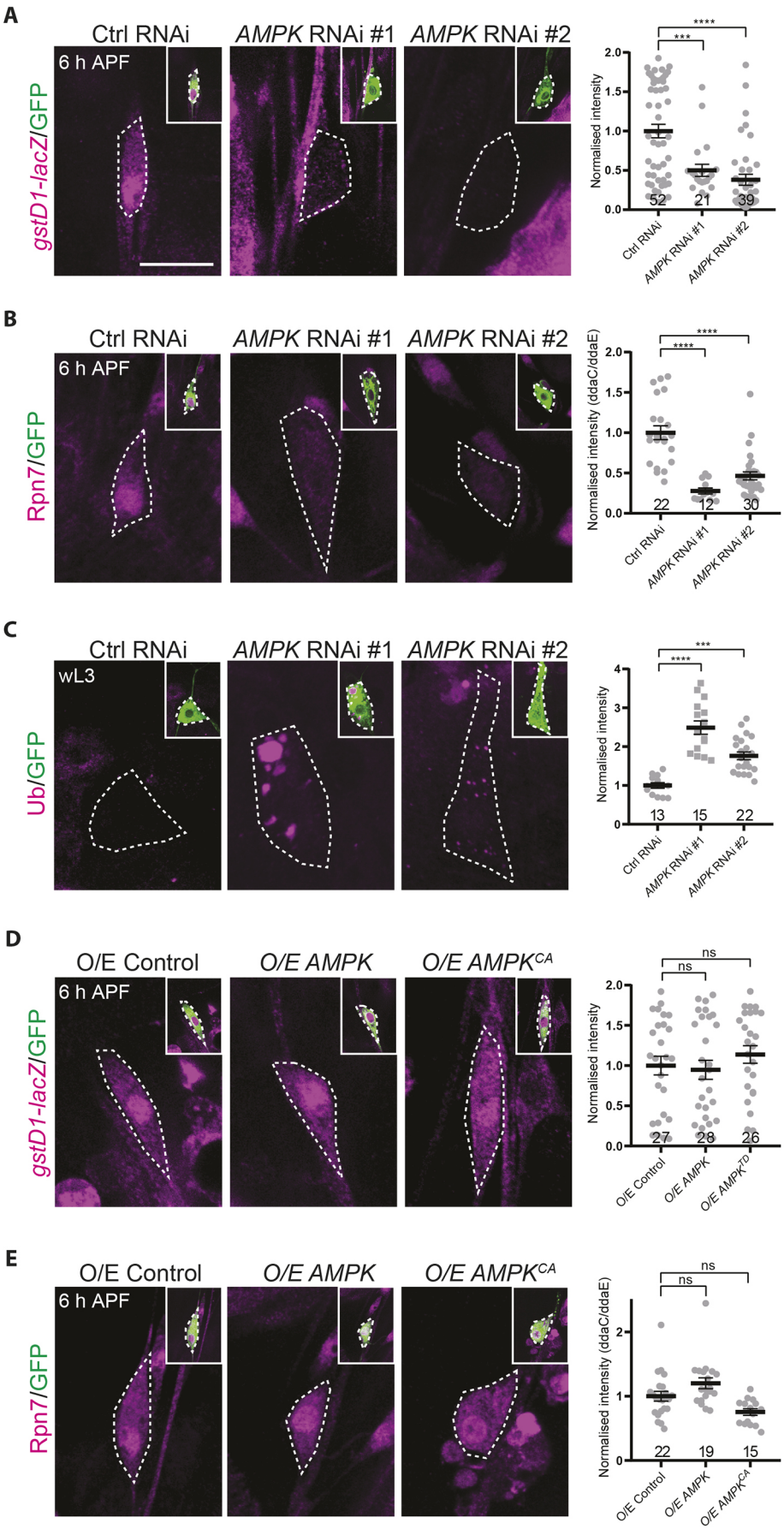

Fig. 3. AMPK is required for activation of the Nrf2-Keap1 pathway prior to dendrite pruning. (A-C) Levels of *gstD1-lacZ* (A), Rpn7 (B) and ubiquitinated protein aggregates (C) in control RNAi, *AMPK* RNAi #1, and *AMPK* RNAi #2 ddaC neurons. (D,E) Expression of *gstD1-lacZ* (D) and Rpn7 (E) in AMPK- and AMPK^{CA}-overexpressing ddaC neurons at 6 h APF. ddaC somata are marked by dashed lines. Insets show GFP-labelled ddaC neurons. Quantitative analyses of normalised fluorescence are shown on the right. Error bars represent s.e.m. One-way ANOVA with Bonferroni test was applied to determine significance for multiple-group comparison. ns, not significant; ***P<0.001, ****P<0.0001. The number of neurons (n) examined in each group is shown on the bars. Scale bar: 10 µm.

Development (2022) 149, dev200536. doi:10.1242/dev.200536

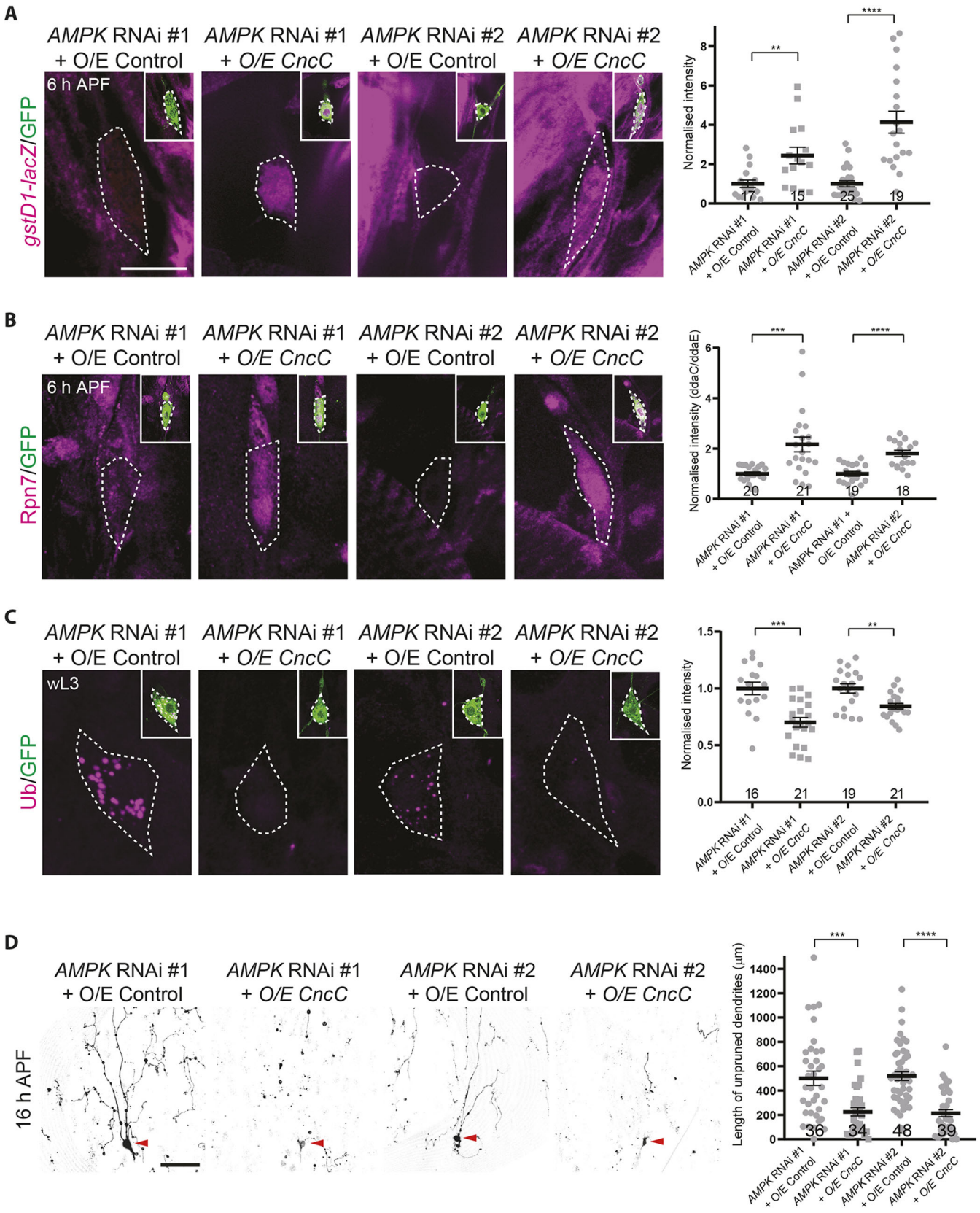

Fig. 4. AMPK regulates dendrite pruning at least partly by activating the Nrf2-Keap1 pathway. (A-C) Levels of *gstD1-lacZ* (A), Rpn7 (B) and ubiquitinated protein aggregates (C) in *AMPK* RNAi #1 or #2 ddaC neurons overexpressing control or CncC. ddaC somata are marked by dashed lines. Insets show GFP-labelled ddaC neurons. (D) Dendrites of ddaC neurons co-expressing *AMPK* RNAi #1 or #2 with control or CncC at 16 h APF. Quantitative analyses of normalised *gstD1-lacZ* (A), Rpn7 (B) and ubiquitinated protein aggregates (C) fluorescence, and length of unpruned dendrites (D) are shown on the right. Red arrowheads point to the somata of ddaC neurons. Error bars represent s.e.m. Two-tailed Student's *t*-test was used to determine statistical significance for pairwise comparison. ***P*<0.01, ****P*<0.001, *****P*<0.0001. The number of neurons (*n*) examined in each group is shown on the bars. Scale bars: 10 μm (A); 50 μm (D).

Development (2022) 149, dev200536. doi:10.1242/dev.200536

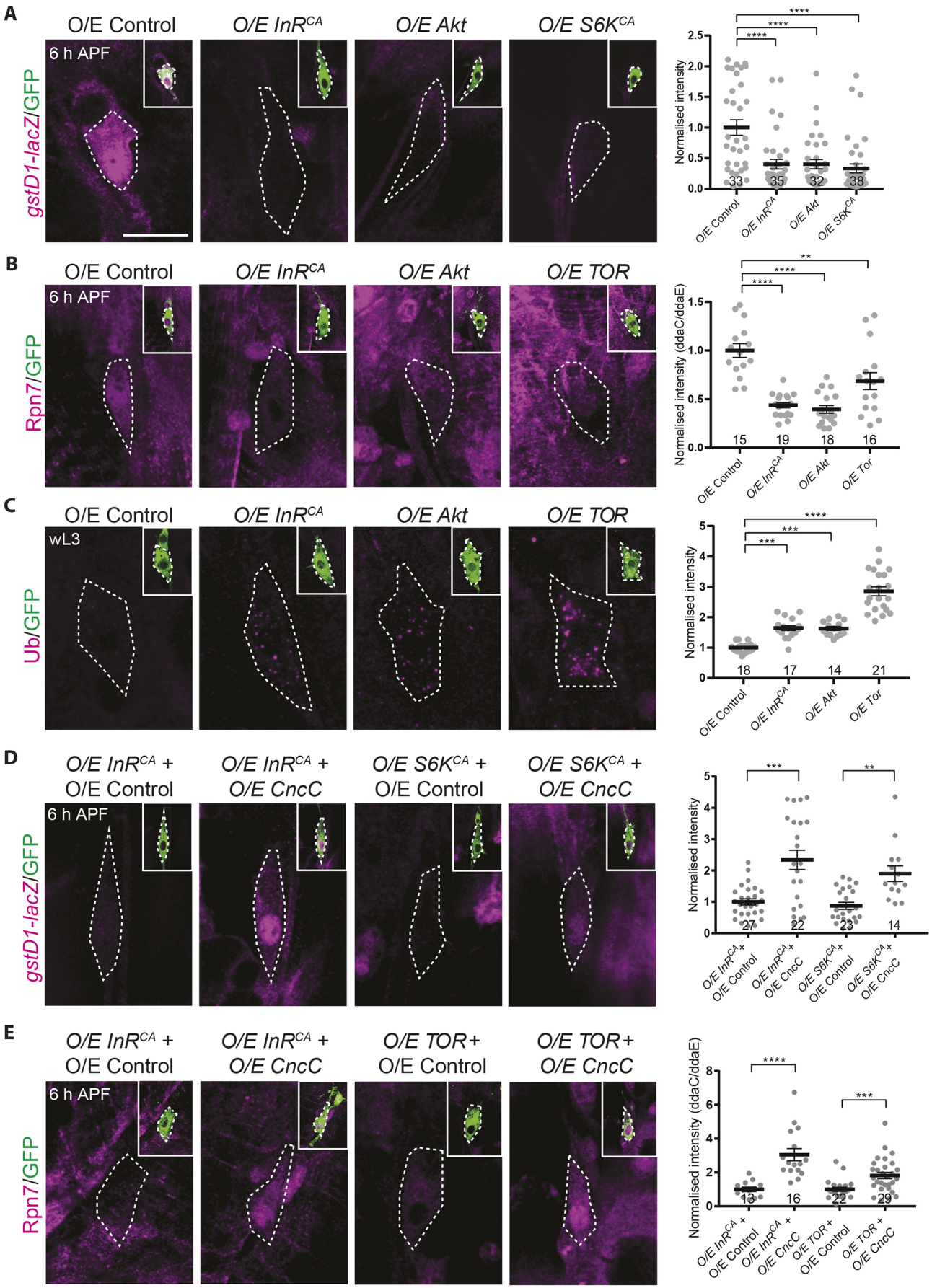

Fig. 5. See next page for legend.

Development (2022) 149, dev200536. doi:10.1242/dev.200536

Fig. 5. The insulin pathway negatively regulates the Nrf2-Keap1 pathway during dendrite pruning. (A-C) Levels of *gstD1-lacZ* (A), Rpn7 (B) and ubiquitinated protein aggregates (C) in control, InR^{CA}-, Akt-, $S6K^{CA}$- or TOR-overexpressing ddaC neurons. (D,E) Expression of *gstD1-lacZ* (D) and Rpn7 (E) in ddaC neurons overexpressing InR^{CA} with control or CncC, overexpressing $S6K^{CA}$/TOR with control or CncC at 6 h APF. ddaC somata are marked by dashed lines. Insets show GFP-labelled ddaC neurons. Quantitative analyses of normalised *gstD1-lacZ* (A,D), Rpn7 (B) and ubiquitinated protein aggregates (C) fluorescence are shown on the right. Error bars represent s.e.m. Two-tailed Student's *t*-test was used to determine statistical significance for pairwise comparison, whereas one-way ANOVA with Bonferroni test was applied to determine significance for multiple-group comparison. ***P*<0.01, ****P*<0.001, *****P*<0.0001. The number of neurons (*n*) examined in each group is shown on the bars. Scale bar: 10 µm.

or #2) (Fig. 4D). This rescue effect was partial because Mical and Hdc expressions remained reduced in these neurons (Fig. S6C). Co-overexpression of CncC and Mical exhibited almost full rescue of the AMPK RNAi phenotypes (Fig. S6D), compared with either Mical or CncC overexpression alone. These data support the conclusion that AMPK regulates dendrite pruning via both Mical and CncC. To confirm that AMPK functions upstream of the Nrf2-Keap1 pathway, we overexpressed AMPK or $AMPK^{CA}$ in CncC RNAi ddaC neurons. Overexpression of AMPK or $AMPK^{CA}$ did not rescue the defects in proteasomal degradation and dendrite pruning in CncC RNAi neurons (Fig. S6E,F), in line with the conclusion that AMPK functions upstream to activate the Nrf2-Keap1 pathway during dendrite pruning. Taken together, our data demonstrate that AMPK is required for activation of the Nrf2-Keap1 pathway, in addition to Mical and Hdc expression, to promote dendrite pruning in ddaC neurons.

The insulin pathway negatively regulates the Nrf2-Keap1 pathway during dendrite pruning

Our previous study indicates that ecdysone signalling is required for activation of the Nrf2-Keap1 pathway during dendrite pruning (Chew et al., 2021). Ecdysone signalling also promotes dendrite pruning by antagonising the insulin pathway, a metabolic pathway (Wong et al., 2013). Attenuation of the insulin pathway during the nonfeeding larval-pupal transition is required for dendrite pruning (Wong et al., 2013). We hypothesised that during the larval-pupal transition low energy levels may lead to changes in the metabolic state and thereby activation of the Nrf2-Keap1 pathway. We next investigated the relationship between the insulin pathway and the Nrf2-Keap1 pathway. Hyperactivation of the insulin pathway and the downstream Target of Rapamycin (TOR) pathway has been reported to cause dendrite pruning defects in ddaC neurons (Wong et al., 2013). Importantly, we found that hyperactivation of the insulin and TOR pathways also led to inhibition of the Nrf2-Keap2 pathway prior to dendrite pruning. Overexpression of InR^{CA} or Akt (hyperactivation of the insulin pathway) or TOR/$S6K^{CA}$ (hyperactivation of the TOR pathway) led to decreases in the levels of *gstD1-lacZ* and Rpn7 expression at 6 h APF compared with their respective controls (Fig. 5A,B). Concomitantly, ubiquitylated protein aggregates were present in InR^{CA}-, Akt- or TOR-overexpressing ddaC neurons (Fig. 5C). These data indicate that the insulin pathway inhibits the Nrf2-Keap1 pathway prior to dendrite pruning, suggesting that attenuation of the insulin pathway is required for activation of the Nrf2-Keap1 pathway. However, hyperactivation of the insulin-TOR pathway did not affect the upregulation of Mical expression in ddaC neurons at the WP stage (Fig. S7A), similar to observations in *CncC* mutant neurons lacking the Nrf2-Keap1 pathway (Chew et al., 2021). These data suggest that the insulin-TOR pathway regulates dendrite pruning in parallel with the Mical pathway. We next examined whether inhibition of the insulin-TOR pathway leads to hyperactivation of the Nrf2-Keap1 pathway. Overexpression of dominant-negative InR (InR^{DN}), dominant-negative phosphoinositide 3-kinase ($PI3K^{DN}$) or Akt RNAi (inhibition of the insulin pathway) or dominant-negative S6K ($S6K^{DN}$) (inhibition of the TOR pathway) did not augment the expression levels of *gstD1-lacZ* and Rpn7 at 6 h APF (Fig. S7B,C), suggesting that inhibition of the insulin pathway is not sufficient for activation of the Nrf2-Keap1 pathway in ddaC neurons.

To verify whether hyperactivation of the insulin pathway inhibits dendrite pruning by antagonising the Nrf2-Keap1 pathway, we co-overexpressed CncC in InR^{CA}- or $S6K^{CA}$-expressing ddaC neurons. Overexpression of CncC significantly restored the expression of *gstD1-lacZ* and Rpn7 in InR^{CA} or $S6K^{CA}$/TOR-expressing neurons compared with their respective controls (Fig. 5D,E). As controls, overexpression of $PI3K^{DN}$ (inhibition of the insulin pathway) or TOR^{TED} (toxic effector domain of TOR)/$S6K^{DN}$ (inhibition of the TOR pathway) did not rescue the defects in proteasome degradation and dendrite pruning in CncC RNAi neurons (Fig. S8A,B). These data are consistent with the notion that the insulin pathway functions upstream to antagonise the Nrf2-Keap1 pathway. In summary, we demonstrate that during the larval-pupal transition downregulation of the insulin pathway is required to activate the Nrf2-Keap1 pathway and, in turn, the proteasomal degradation pathway to promote dendrite pruning.

We and others have reported that PP2A is required for regulation of dendrite pruning (Rui et al., 2020; Wolterhoff et al., 2020); moreover, the AMPK-PP2A axis antagonises the insulin pathway in the fly and silkworm fat body (Yuan et al., 2020). Interestingly, when the catalytic subunit (Microtubule star, Mts) or the scaffold subunit (PP2A-29B) was compromised in ddaC neurons, neither *gstD1-lacZ* nor Rpn7 expression levels were affected at 6 h APF (Fig. S9A,B). Consistent with this, no ubiquitylated protein aggregates were observed in *mts* RNAi or *Pp2A-29B* RNAi neurons (Fig. S9C). Thus, unlike AMPK, PP2A regulates dendrite pruning independently of Nrf2-Keap1 pathway activation.

AMPK promotes dendrite pruning at least partly by inhibiting the insulin pathway

Given that loss of AMPK function phenocopies hyperactivation of the insulin-TOR pathway, we next examined whether AMPK promotes dendrite pruning by inhibition of the insulin pathway. When the insulin pathway was inhibited by overexpressing InR^{DN} (Fig. 6B,K,L), $PI3K^{DN}$ (Fig. 6C,K,L) or Akt RNAi (Fig. 6E,K,L) in AMPK RNAi ddaC neurons, dendrite pruning defects were significantly suppressed at 16 h APF compared with their respective controls (Fig. 6A,D,K,L). When the TOR pathway was inactivated by overexpressing TSC1-TSC2 (Fig. 6G,K,L), TOR^{TED} (Fig. 6H,K,L), $S6K^{DN}$ (Fig. 6I,K,L) or 4E-BP(AA) (Fig. 6J-L) in AMPK RNAi ddaC neurons, the dendrite pruning defects were also partially rescued. The numbers of major dendrites remained unaltered in those ddaC neurons at the WP stage (Fig. 6A-J, Fig. S10A). However, Mical levels were not restored in these neurons (Fig. S10B,B′). Importantly, co-overexpression of InR^{DN} and Mical almost completely rescued the AMPK RNAi phenotypes compared with either Mical or InR^{DN} overexpression alone (Fig. S10C). These data support the notion that AMPK regulates dendrite pruning via both the Mical and the insulin pathway. As controls, when $AMPK^{CA}$ was co-overexpressed with InR^{CA} or TOR in ddaC neurons, the dendrite pruning defects were not rescued (Fig. S10D), consistent with the notion that AMPK functions upstream to

Development (2022) 149, dev200536. doi:10.1242/dev.200536

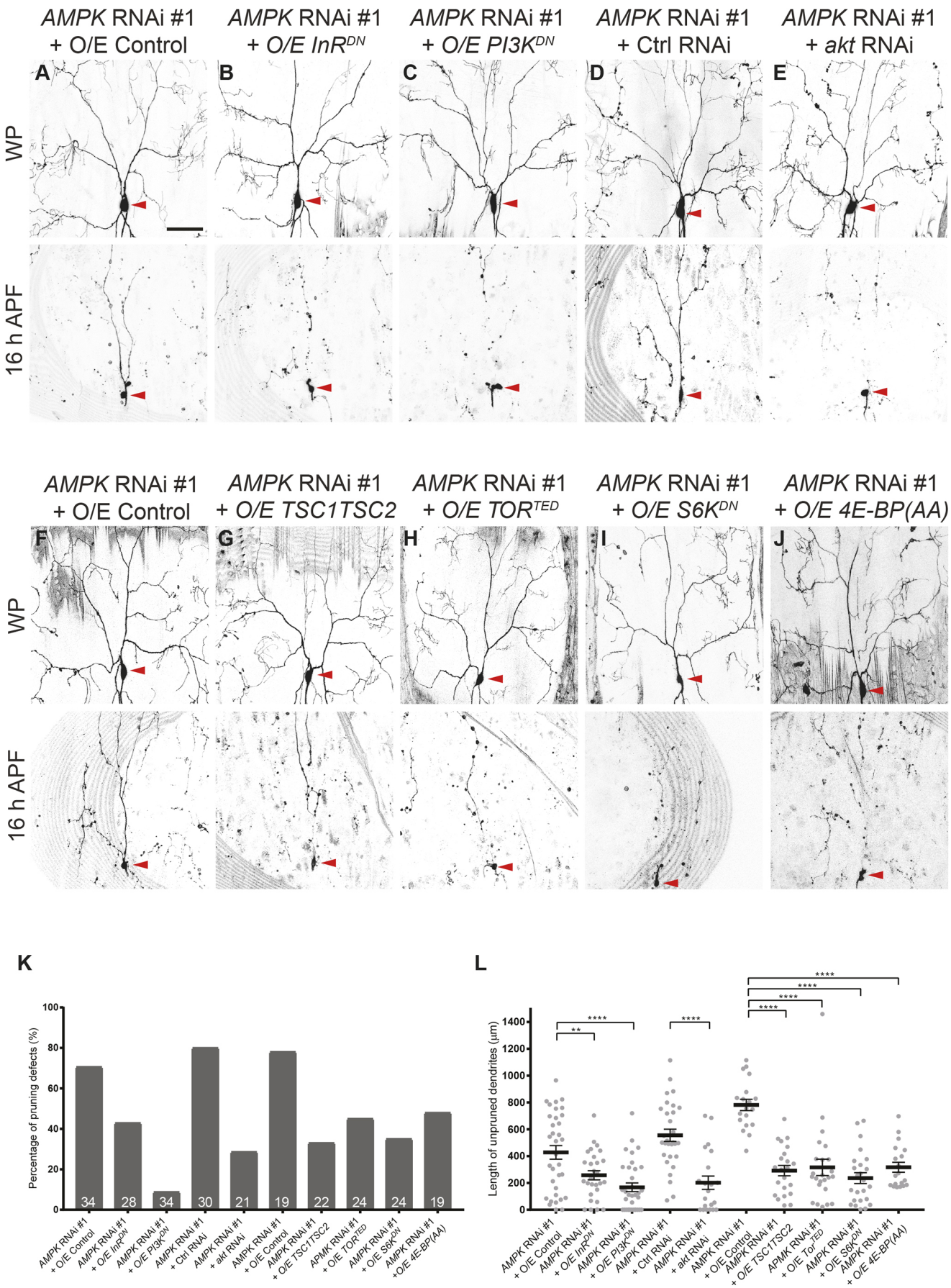

Fig. 6. See next page for legend.

Development (2022) 149, dev200536. doi:10.1242/dev.200536

Fig. 6. AMPK promotes dendrite pruning at least partly by inhibiting the insulin pathway. (A-J) Dendrites of *AMPK* RNAi #1 ddaC neurons overexpressing control (A,F), InR^{DN} (B), PI3K^{DN} (C), control RNAi (D), *Akt* RNAi (E), TSC1, TSC2 (G), TOR^{TED} (H), S6K^{DN} (I) and 4E-BP(AA) (J) at WP and 16 h APF stages. Red arrowheads point to the somata of ddaC neurons. (K) Percentages of ddaC neurons showing the dendrite pruning defects at 16 h APF. (L) Quantitative analysis of unpruned dendrite length at 16 h APF. Error bars represent s.e.m. Two-tailed Student's *t*-test was used to determine statistical significance for pairwise comparison, whereas one-way ANOVA with Bonferroni test was applied to determine significance for multiple-group comparison. ***P*<0.01, *****P*<0.0001. The number of neurons (*n*) examined in each group is shown on the bars. Scale bar: 50 µm.

antagonise the insulin-TOR pathway during dendrite pruning. In addition, Akt RNAi or TOR^{TED} overexpression did not rescue the dendrite pruning defects in Mts^{DN}-expressing ddaC neurons (Fig. S9D), further confirming that PP2A regulates dendrite pruning independently of the insulin-TOR pathway.

Taken together, our data strongly suggest that the AMPK-insulin pathway is required to activate the Nrf2-Keap1 pathway, thereby promoting dendrite pruning.

The AMPK-insulin pathway axis is required for ecdysone signalling to activate the Nrf2-Keap1 pathway

We next examined whether AMPK is required for ecdysone signalling to activate its downstream pathways to promote dendrite pruning. To this end, we knocked down AMPK in Sox14-overexpressing ddaC neurons and examined activation of the Nrf2-Keap1 pathway at 6 h APF. Sox14 overexpression has been previously shown to promote precocious activation of ecdysone signalling and accelerate dendrite pruning (Kirilly et al., 2009). Sox14 overexpression also led to precocious activation of the Nrf2-Keap1 pathway, as the expression of *gstD1-lacZ* and Rpn7 was elevated at 3 h and 6 h APF (Chew et al., 2021) (Fig. 2D, Fig. S4C). When AMPK was knocked down in Sox14-overexpressing ddaC neurons, *gstD1-lacZ* and Rpn7 expression was significantly downregulated at 6 h APF (Fig. 7A,B), suggesting that activation of the Nrf2-Keap1 pathway by Sox14 overexpression requires AMPK. Likewise, hyperactivation of the insulin pathway also suppressed the Nrf2-Keap1 pathway in Sox14-overexpressing ddaC neurons. Overexpression of InR^{CA} or Akt (hyperactivation of the insulin pathway) led to reductions in *gstD1-lacZ* and Rpn7 expression in Sox14-overexpressing ddaC neurons compared with Sox14-overexpressing controls (Fig. 7A,B). These data suggest that ecdysone signalling antagonises the insulin pathway to promote the Nrf2-Keap1 pathway prior to dendrite pruning. Finally, the precocious dendrite pruning induced by Sox14 overexpression was significantly suppressed by AMPK RNAi or by InR^{CA} or Akt overexpression at 6 h APF (Fig. 7C). Collectively, these genetic data further indicate that the AMPK-insulin pathway axis is required for ecdysone signalling to activate the Nrf2-Keap1 pathway and thereby induce dendrite pruning.

In summary, we show that the metabolic regulator AMPK activates the Nrf2-Keap1 pathway and Mical expression in response

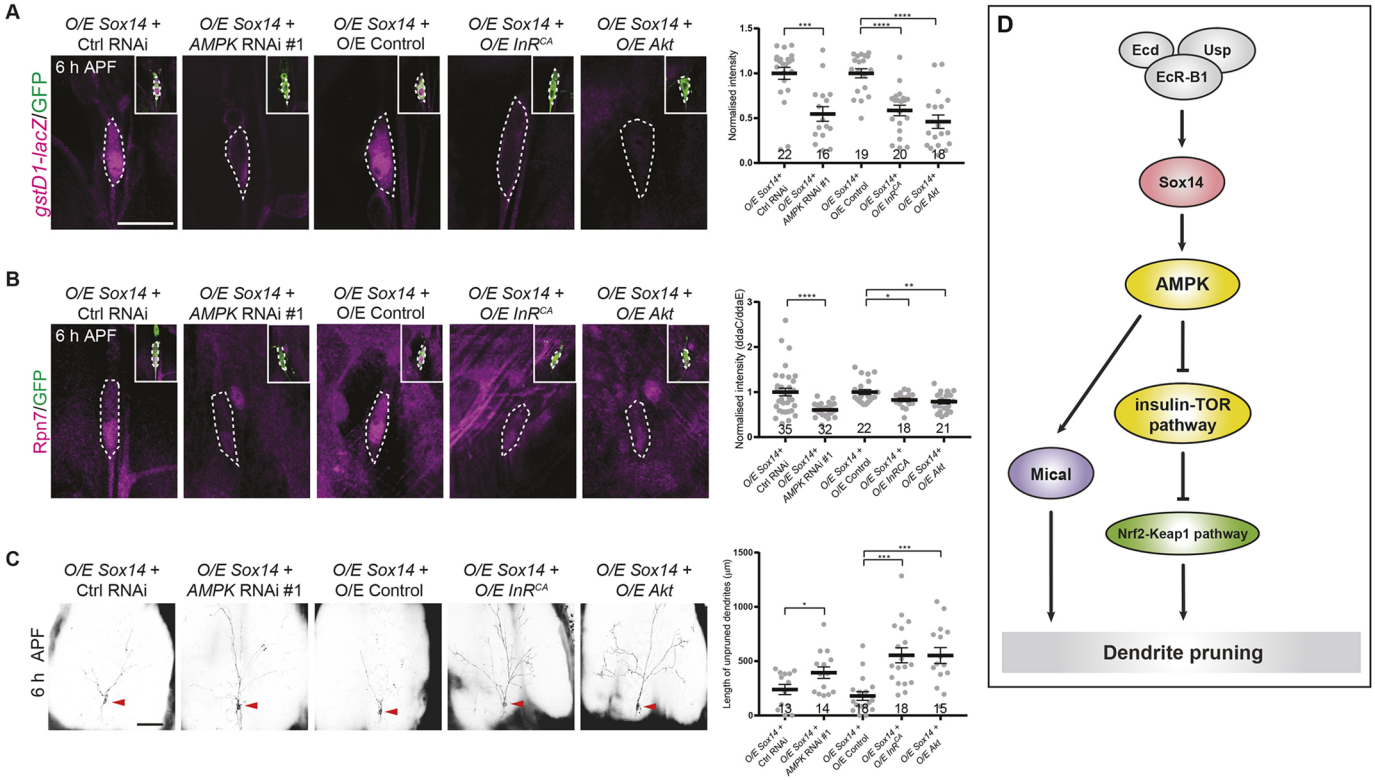

Fig. 7. The AMPK-insulin pathway axis is required for Sox14 to activate the Nrf2-Keap1 pathway. (A,B) Expression of *gstD1-lacZ* (A) and Rpn7 (B) in Sox14-overexpressing ddaC neurons co-expressing control RNAi, *AMPK* RNAi, control, InR^{CA} and Akt. ddaC somata are marked by dashed lines. Insets show GFP-labelled ddaC neurons. (C) Dendrites of Sox14-overexpressing ddaC neurons co-expressing control RNAi, *AMPK* RNAi, control, InR^{CA} and Akt. Red arrowheads point to the somata of ddaC neurons. Quantitative analyses of normalised *gstD1-lacZ* (A) and Rpn7 (B) fluorescence and unpruned dendrite length (C) are shown on the right. Error bars represent s.e.m. Two-tailed Student's *t*-test was used to determine statistical significance for pairwise comparison, whereas one-way ANOVA with Bonferroni test was applied to determine significance for multiple-group comparison. **P*<0.05, ***P*<0.01, ****P*<0.001, *****P*<0.0001. The number of neurons (*n*) examined in each group is shown on the bars. (D) Schematic of the proposed working model. The metabolic regulator AMPK activates the Nrf2-Keap1 pathway and Mical expression downstream of EcR-B1/Usp and Sox14; moreover, AMPK activates the Nrf2-Keap1 pathway and promotes dendrite pruning by antagonizing the insulin-TOR pathway. Scale bars: 10 µm (A); 50 µm (C).

Development (2022) 149, dev200536. doi:10.1242/dev.200536

to ecdysone during the larval-pupal transition; moreover, our genetic data indicate that AMPK activates the Nrf2-Keap1 pathway and promotes dendrite pruning by antagonising the insulin pathway (see the model in Fig. 7D).

DISCUSSION

AMPK regulates Mical and Hdc expression and the Nrf2-Keap1 pathway during dendrite pruning

AMPK is a key metabolic regulator that maintains energy homeostasis in eukaryotes (Hardie et al., 2012; Trefts and Shaw, 2021). In *Drosophila*, AMPK expression and activity are activated in the fat body in response to the hormone ecdysone (Yuan et al., 2020). In this study, we identify AMPK as an important player in dendrite pruning during *Drosophila* metamorphosis. We provide multiple lines of genetic evidence demonstrating a cell-autonomous role of AMPK in dendrite pruning of ddaC neurons. Importantly, AMPK regulates dendrite pruning via both Mical and Hdc expression and activation of the Nrf2-Keap1 pathway. When AMPK function was compromised, the expression levels of Mical were strongly reduced in ddaC neurons. AMPK is also required to upregulate expression of the *mical1-lacZ* reporter. Our data suggest that AMPK likely regulates Mical transcription. Interestingly, AMPK is dispensable for expression of EcR and Sox14, highlighting a specific role of AMPK in the regulation of Mical and Hdc expression. One possibility is that EcR and Sox14 are ecdysone primary-response genes (Beckstead et al., 2005; Karim and Thummel, 1992), and their expression might depend mainly on ecdysone and its nuclear receptors.

Our previous study demonstrated that the Nrf2-Keap1 pathway is activated by ecdysone signalling to promote proteasomal degradation activity prior to dendrite pruning (Chew et al., 2021). Compared with Sox14, Mical and Hdc expression at the WP stage, the expression of CncC (Nrf2) and the reporter *gstD1-lacZ* is upregulated at 6 h APF (Chew et al., 2021; Kirilly et al., 2009; Loncle and Williams, 2012), suggesting that among these ecdysone-response targets, the Nrf2-Keap1 pathway is the most downstream pathway induced by ecdysone signalling. However, how the Nrf2-Keap1 pathway is activated prior to dendrite pruning was poorly understood. We show here that AMPK plays an important role in activation of the Nrf2-Keap1 pathway, in addition to regulation of Mical and Hdc expression. As the Nrf2-Keap1 pathway can activate the antioxidant response pathway and the proteasomal degradation pathway during dendrite pruning (Chew et al., 2021), we made use of both the *gstD1-lacZ* reporter and the proteasomal subunit Rpn7 to detect activation of the Nrf2-Keap1 pathway. With both reporters, we unambiguously demonstrate that AMPK is required but not sufficient to induce the downstream targets of the Nrf2-Keap1 pathway. Overexpression of CncC significantly rescued AMPK RNAi defects in terms of *gstD1-lacZ* and Rpn7 expression and dendrite pruning, whereas AMPK or $AMPK^{CA}$ overexpression did not rescue CncC RNAi defects. Collectively, these genetic data strongly suggest that AMPK acts upstream to promote the Nrf2-Keap1 pathway and dendrite pruning. Although mammalian AMPK has been reported to facilitate nuclear accumulation of Nrf2 in cultured cells (Joo et al., 2016), we observed no alteration in nuclear enrichment of CncC (fly Nrf2) in ddaC neurons at 6 h APF (Fig. S5A). This suggests a potential role of AMPK in facilitating CncC transcriptional activity, instead of its nuclear accumulation, in fly. Furthermore, the Sox14 overexpression data indicate that AMPK is required for ecdysone signalling to activate the Nrf2-Keap1 pathway. Thus, our genetic evidence supports a model in which the metabolic regulator AMPK acts downstream of ecdysone signalling to induce the Nrf2-Keap1 pathway during dendrite pruning. In support of this model, AMPK expression or activity is elevated in the fat body by ecdysone signalling (Yuan et al., 2020).

AMPK promotes the Nrf2-Keap1 pathway and dendrite pruning partly by inhibition of the insulin pathway

In mammals, AMPK counteracts the insulin-TOR pathway by inhibiting either Akt or mTORC1 activity (González et al., 2020; Gwinn et al., 2008; Kim et al., 2009). In fly and silkworm, AMPK activates PP2A, which in turn dephosphorylates InR and Akt in the fat body; this AMPK-PP2A axis antagonises the insulin-TOR pathway to reduce food consumption and suppress the growth rate (Yuan et al., 2020). We have provided multiple lines of genetic evidence showing that AMPK activates the Nrf2-Keap1 pathway and promotes dendrite pruning at least partly by inhibiting the insulin-TOR pathway during dendrite pruning. First, hyperactivation of the insulin-TOR pathway led to reductions in *gstD1-lacZ* and Rpn7 expression prior to dendrite pruning, indicative of an impaired Nrf2-Keap1 pathway. This suggests antagonism between these two pathways. Second, overexpression of CncC restored the expressions of *gstD1-lacZ* and Rpn7 in InR^{CA}, $S6K^{CA}$ or TOR-overexpressing ddaC neurons with a hyperactive insulin-TOR pathway. Consistent with this, attenuation of the insulin-TOR pathway by $PI3K^{DN}$, TOR^{TED} or $S6K^{DN}$ did not rescue the defects in CncC RNAi ddaC neurons. These data suggest that the insulin-TOR pathway functions upstream to suppress the Nrf2-Keap1 pathway. Finally, attenuation of the insulin-TOR pathway strongly suppressed the dendrite pruning defects associated with AMPK RNAi knockdown, whereas overexpression of active AMPK did not suppress the dendrite pruning defects in InR^{CA} or TOR-overexpressing neurons. Taken together, these genetic data strongly support the conclusion that AMPK acts upstream to inhibit the insulin-TOR pathway, thus activating the Nrf2-Keap1 pathway during dendrite pruning (Fig. 7D). Interestingly, AMPK regulates dendrite pruning independently of PP2A. Unlike AMPK, PP2A is not required for activation of the Nrf2-Keap1 pathway during dendrite pruning. Moreover, attenuation of the insulin-TOR pathway by *Akt* RNAi or TOR^{TED} did not suppress the *PP2A* defects. Thus, unlike observations in fat body, the AMPK-PP2A axis does not exist during dendrite pruning of ddaC neurons, suggesting that its function is context dependent. Moreover, the Cullin1-based E3 ligase has previously been shown to inactivate the insulin pathway by ubiquitylating Akt to promote dendrite pruning (Wong et al., 2013). Therefore, AMPK and Cullin1 E3 ligase might act as double brakes to ensure complete and rapid inactivation of the insulin pathway during the larval-pupal transition, thereby facilitating dendrite pruning.

How is the Nrf2-Keap1 pathway activated by ecdysone signalling during the nonfeeding prepupal stage? At the late larval stage, ecdysone acts directly on the insect larval central nervous system to induce larval wandering behaviour and enable larva to move away from food (Dominick and Truman, 1985, 1986). It reduces feeding behaviour and food consumption, which leads to lipolysis in the fat body (Wang et al., 2010). As a result, ecdysone-induced wandering behaviour can cause energy deprivation and increase the cellular AMP/ATP ratio, which in turn leads to activation of AMPK and subsequent downregulation of the insulin-TOR pathway (Colombani et al., 2005; Yuan et al., 2020). Likewise, in ddaC neurons ecdysone signalling might also activate AMPK in response to low energy levels, which in turn attenuates the insulin-TOR pathway to suppress anabolism, such as protein/lipid synthesis, during the larval-pupal transition. It is conceivable that attenuation of the insulin pathway may directly or indirectly activate the Nrf2-

Development (2022) 149, dev200536. doi:10.1242/dev.200536

Keap1 pathway. In support of this possibility, worm Akt kinases directly phosphorylate the worm Nrf2/CncC counterpart SKN-1; reduced insulin pathway activity leads to increased SKN-1 nuclear accumulation and thereby SKN-1 target gene expression (Tullet et al., 2008). However, in fly ddaC neurons, we did not observe an increase in the expression of *gstD1-lacZ* or Rpn7, two targets of the Nrf2-Keap1 pathway, when the insulin-TOR pathway was constitutively inhibited. This suggests that attenuation of the insulin pathway is necessary but not sufficient to activate the Nrf2-Keap1 pathway in fly sensory neurons; other pathways might act redundantly with the insulin pathway to modulate activation of the Nrf2-Keap1 pathway during the larval-pupal transition. Further investigations are required to identify those unknown pathways. Activation of the Nrf2-Keap1 pathway leads to upregulation of the proteasomal degradation machinery, which promotes dendrite pruning in ddaC neurons (Chew et al., 2021).

During the preparation of this article, the Rumpf laboratory published another paper showing that AMPK is activated by ecdysone and promotes oxidative phosphorylation, which may allow neurons to generate energy using amino acids (Marzano et al., 2021). They made use of an AMPK sensor to demonstrate that AMPK is activated by ecdysone signalling prior to dendrite pruning, supporting our conclusion that AMPK is required for ecdysone signalling to activate the Nrf2-Keap1 pathway and promote dendrite pruning (see the model in Fig. 7D). Both studies are largely complementary. Their study speculates that AMPK may regulate Mical translation, whereas we report that AMPK regulates Mical expression likely via transcriptional regulation. More importantly, we demonstrate a pathway in which AMPK is required to activate the Nrf2-Keap1 pathway and promote dendrite pruning by attenuation of the insulin pathway. Moreover, hyperactivated mammalian TOR (mTOR) has been reported to correlate with impaired developmental neuronal pruning in layer V pyramidal neurons in individuals with autism-spectrum disorders (Tang et al., 2014). Thus, this study would open new avenues for further study of the mechanisms of the conserved AMPK-insulin-TOR pathway axis and the Nrf2-Keap1 pathway in neuronal remodelling in mammals, including humans.

MATERIALS AND METHODS

Fly strains

All *Drosophila* stocks and crosses were maintained in standard cornmeal media at 25°C. Third instar larvae or early pupae at 0, 3, 6 or 16 h APF (both male and female) were used in this study. *UAS-Mical*^{NT} (non-functional N-terminal Mical fragment as a UAS-control transgene) (Terman et al., 2002), *ppk-Gal4* on II and III chromosome (Grueber et al., 2003), *SOP-flp* (#42) (Matsubara et al., 2011), *ampk*^{D2}, *UAS-AMPK*^{KR} (Lee et al., 2007), *gstD1-lacZ*, *UAS-CncC* (Sykiotis and Bohmann, 2008), *UAS-Sox14* (Kirilly et al., 2009), *UAS-4E-BP*^{4A} (Teleman et al., 2005), *UAS-Mts*^{DN} (Hannus et al., 2002), *mical1-lacZ* (this study).

The following stocks were obtained from Bloomington *Drosophila* Stock Centre (BDSC): *UAS-mCD8::GFP, FRT19A, UAS-Dicer2, tubP-Gal80, AMPK* RNAi #2 (#25931), *Cnc* RNAi #2 (#40854), *Rpn7* RNAi #1 (#34787), *UAS-AMPK* (#32108), *UAS-AMPK*^{CA} (#32110), *UAS-InR*^{CA} (#8263), *UAS-Akt* (#8191), *UAS-S6K*^{CA} (#6914), *UAS-Tor* (#80932), *UAS-PI3K*^{DN} (#25918), *Akt* RNAi (#31701), *UAS-TOR*^{TED} (#7013), *UAS-S6K*^{DN} (#6911), *UAS-InR*^{DN} (#8252), *UAS-TSC1,TSC2* (#80576).

The following stocks were obtained from the Vienna *Drosophila* Resource Centre (VDRC): *AMPK* RNAi #1 (#106200), *Cnc* RNAi #1 (#37674), *Rpn7* RNAi #2 (#101467), *EcR* RNAi (#37058), *Sox14* RNAi (#10856), *Mical* RNAi (#46097), *mts* RNAi (#41924), *pp2a-29b* RNAi (#49671), control RNAi (#25271; *γ-Tub37C*).

Genotypes of the fly strains shown in each figure are listed in Supplementary Materials and Methods.

Generation of the *Mical-lacZ* reporter

A genomic clone, *BACR39F04*, containing the entire *Mical* genomic region was used as a template to amplify four overlapping DNA fragments (*Mical1*, *-2*, *-3*, *-4*), covering around 20 kb of the putative *Mical* regulatory region. These PCR fragments were first inserted into the *pGEM-T* easy vector (Promega) by TA cloning and then subcloned into the *pCaSpeR-hs43-lacZ* vector. Plasmids were sequenced and purified with the QIAGEN Midi Extraction Kit. Transgenic flies were generated by BestGene.

Primers used were: *Mical1* forward: 5′-CACCGCGGCCGCATCGA-CAGCGACTGAGACAA-3′; *Mical1* reverse: 5′-AAAGCGGCCGCAGG-AGAGAGGTTTGGTAGACA-3′; *Mical2* forward: 5′-CACCGCGGCCG-CATGAGGCTGCTGATTAGATGG-3′; *Mical2* reverse: 5′-AAAGCGG-CCGCGCACACTCAACTTACTTGTCTC-3′; *Mical3* forward: 5′-CACC-GCGGCCGCCACGAGTTCTTCGAATTTCG-3′; *Mical3* reverse: 5′-AAAGCGGCCGCACAGCAAACTGCTCAGCCACT-3′; *Mical4* forward: 5′-CACCGCGGCCGCGCTAAGTAGGTGTTTCTTGTC-3′; *Mical4* reverse: 5′-AAAGCGGCCGCTAACTTGCATCTGGTTTCAAC-3′.

Immunohistochemistry and antibodies

Immunohistochemistry was performed using the following antibodies at the indicated dilutions: mouse anti-β-galactosidase (1:1000; Promega, Z378A), mouse Rpn7 (1:500; Santa Cruz Biotechnology, sc-65750), mouse anti-Ubiquitin (1:500; FK2, Enzo Life Sciences, BML-PW8810), mouse anti-Futsch [1:50, Developmental Studies Hybridoma Bank (DSHB), 22C10], mouse anti-EcR-B1 (1:50; DSHB, AD4.4), mouse anti-Sox14 (1:500; produced in the Yu lab), guinea pig anti-Mical (1:500; Kirilly et al., 2009), mouse anti-CncC (P2) (1:500; Chew et al., 2021), and mouse anti-Hdc (1:5; DSHB, U33). Cy3- or Cy5-conjugated secondary antibodies (Jackson ImmunoResearch, 115-165-003, 106-165-003 and 123-605-021) were used at 1:500. For normal immunostaining, staged pupae or larvae were dissected in cold PBS and fixed with 4% formaldehyde for 20 min. For Futsch immunostaining, wL3 larvae were dissected in Ca^{2+}-free HL3.1 saline and subsequently fixed for 15 min in freshly prepared PHEM fixation buffer containing 0.25% glutaraldehyde, 4% formaldehyde and 0.1% Triton X-100. After fixation, the samples were quenched in 50 mM ammonium chloride for 5 min (Witte et al., 2008). Control and mutant samples were incubated simultaneously in the same tubes. Samples were mounted in VectaShield mounting medium, and directly visualised using an Olympus FV3000 confocal microscope. The images were taken using the same confocal setting within the same set of the experiments, and the data were processed in parallel. The experiments were repeated at least twice.

Live imaging analysis

To image the dendrites of ddaC sensory neurons at WP or 6 h APF, pupae were briefly rinsed with PBS buffer, followed by immersion in 80% glycerol. To image da neurons at 16 h APF, pupal cases were removed before being mounted with 80% glycerol. Images of da neurons were taken on a Leica SPE2 laser confocal microscope.

MARCM analysis of da sensory neurons

MARCM clonal analysis, dendrite imaging and quantification were carried out as previously described (Kirilly et al., 2009). ddaC clones were identified based on their location and morphology at WP stage. ddaC neurons were then examined for dendrite pruning defects at 16 h APF.

Live imaging of EB1-GFP comet

Larvae (96 h AEL) expressing *UAS-EB1-GFP* driven by the *Gal4*$^{4-77}$ driver were mounted with halocarbon oil (Santa Cruz Biotechnology, sc-250077) onto slides for time-lapse imaging. EB1-GFP comets were visualised using an Olympus FV3000 confocal microscope with 60× oil lens, 3× zoom and 125 frames of 6-*z*-step images were taken within 3 min (at 1.45 s intervals). Kymographs were generated from *z*-projected time-lapse images using the ImageJ plugin KymographBuilder.

Quantification of dendrites

Live confocal images of da neurons expressing *mCD8-GFP* were conducted at the WP stage or at 16 h APF, as described previously (Chew et al., 2021).

Development (2022) 149, dev200536. doi:10.1242/dev.200536

Dorsal is up in all images. For wild-type or mutant ddaC neurons, the percentages of pruning defects were quantified in a 275 µm×275 µm region of the dorsal dendritic area, originating from the abdominal segments 2-4. The pruning defects include both severing and fragmentation defects, which were determined by the following criteria. The severing defect was determined by the presence of dendrites that remained attached to the soma at 16 h APF, whereas the dendrite fragmentation defect was defined as the presence of dendrite branches near the ddaC territory but which were severed from their proximal parts at 16 h APF (Fig. 1A). The total length of unpruned dendrites was measured in a 275 µm×275 µm region of the dorsal dendritic field using ImageJ. The number of neurons (*n*) examined in each group is shown on the bars. GraphPad Prism software was used to generate plots of average length and s.e.m.

Quantification of immunostaining

Images of da sensory neurons were taken from projected *z*-stacks (at 1.5 µm intervals) using an Olympus FV3000 confocal microscope. To measure fluorescence intensities, cell nuclei (CncC, Rpn7, *gstD1-lacZ*, EcR-B1, Sox14 and *mical1-lacZ* immunostaining) or whole soma (Ub, Mical and Hdc immunostaining) contours were drawn based on the GFP channel in ImageJ. To quantify the fluorescence intensities of *gstD1-lacZ*, Ub and *mical1-lacZ*, after subtracting the background (Rolling Ball Radius=50) on the entire image of that channel, the mean grey values in the marked area in ddaC neurons were measured. To measure the fluorescence intensities of CncC, Rpn7, EcR-B1, Sox14, Mical and Hdc after subtracting the background (Rolling Ball Radius=50) on the entire image of that channel, the mean grey value in the marked area in ddaC and ddaE on the same images were measured and their ratios were calculated. The values were normalised to the corresponding average control values and subjected to statistical analysis for comparison between different conditions. Graphs display the average values of the normalised intensities (*gstD1-lacZ*, Ub and *Mical-lacZ*) or ddaC/ddaE ratios (CncC, Rpn7, EcR-B1, Sox14, Mical and Hdc) and s.e.m. normalised to the controls.

To quantify Futsch immunostaining in the dendrites, fluorescence intensities of Futsch/HRP in 20 µm of major dorsal dendrites that were 30 µm away from the centre of the soma were measured, and their ratios were calculated.

The experiments were repeated twice. The number of ddaC neurons (*n*) examined in each group is shown on the bars. Insets show ddaC neurons labelled by *ppk-Gal4*-driven mCD8-GFP expression staining. Dorsal is up in all images.

Statistical analysis

For pairwise comparison, two-tailed Student's *t*-test was used to determine statistical significance. For multiple-group comparison, one-way ANOVA with Bonferroni test was applied to determine significance. Error bars in all graphs represent s.e.m. Statistical significance was defined as ****P<0.0001, ***P<0.001, **P<0.01, *P<0.05. The number of neurons (*n*) in each group is shown on the bars. All quantitative data are included in Table S1.

Acknowledgements

We thank D. Bohmann, Y. Jan, H. Jasper, A. L. Kolodkin, T. Uemura, the BDSC, the DSHB (University of Iowa) and the VDRC (Austria) for generously providing antibodies and fly stocks. We thank W. L. Yong and M. Rui for assistance and other Yu lab members for helpful discussions.

Competing interests

The authors declare no competing or financial interests.

Author contributions

Conceptualization: L.Y.C., S.L., F.Y.; Methodology: L.Y.C., J.H., J.J.L.W.; Formal analysis: L.Y.C., J.J.L.W.; Investigation: L.Y.C., J.H., J.J.L.W.; Resources: L.Y.C., S.L.; Data curation: L.Y.C., J.H., J.J.L.W.; Writing - original draft: L.Y.C., F.Y.; Supervision: S.L., F.Y.; Project administration: F.Y.; Funding acquisition: F.Y.

Funding

F.Y. is funded by Temasek Life Sciences Laboratory Singapore (TLL-2040) and National Research Foundation Singapore (SBP-P3 and SBP-P8).

Peer review history

The peer review history is available online at https://journals.biologists.com/dev/article-lookup/doi/10.1242/dev.200536.

References

Alyagor, I., Berkun, V., Keren-Shaul, H., Marmor-Kollet, N., David, E., Mayseless, O., Issman-Zecharya, N., Amit, I. and Schuldiner, O. (2018). Combining developmental and perturbation-seq uncovers transcriptional modules orchestrating neuronal remodeling. *Dev. Cell* **47**, 38-52.e36. doi:10.1016/j.devcel.2018.09.013

Beckstead, R. B., Lam, G. and Thummel, C. S. (2005). The genomic response to 20-hydroxyecdysone at the onset of Drosophila metamorphosis. *Genome Biol.* **6**, R99. doi:10.1186/gb-2005-6-12-r99

Boulanger, A., Clouet-Redt, C., Farge, M., Flandre, A., Guignard, T., Fernando, C., Juge, F. and Dura, J.-M. (2011). ftz-f1 and Hr39 opposing roles on EcR expression during Drosophila mushroom body neuron remodeling. *Nat. Neurosci.* **14**, 37-44. doi:10.1038/nn.2700

Bu, S., Yong, W. L., Lim, B. J. W., Kondo, S. and Yu, F. (2021). A systematic analysis of microtubule-destabilizing factors during dendrite pruning in Drosophila. *EMBO Rep.* **22**, e52679. doi:10.15252/embr.202152679

Chew, L. Y., Zhang, H., He, J. and Yu, F. (2021). The Nrf2-Keap1 pathway is activated by steroid hormone signaling to govern neuronal remodeling. *Cell Rep.* **36**, 109466. doi:10.1016/j.celrep.2021.109466

Colombani, J., Bianchini, L., Layalle, S., Pondeville, E., Dauphin-Villemant, C., Antoniewski, C., Carré, C., Noselli, S. and Léopold, P. (2005). Antagonistic actions of ecdysone and insulins determine final size in Drosophila. *Science* **310**, 667-670. doi:10.1126/science.1119432

Consoulas, C., Duch, C., Bayline, R. J. and Levine, R. B. (2000). Behavioral transformations during metamorphosis: remodeling of neural and motor systems. *Brain Res. Bull.* **53**, 571-583. doi:10.1016/S0361-9230(00)00391-9

Dominick, O. S. and Truman, J. W. (1985). The physiology of wandering behaviour in Manduca sexta. II. The endocrine control of wandering behaviour. *J. Exp. Biol.* **117**, 45-68. doi:10.1242/jeb.117.1.45

Dominick, O. S. and Truman, J. W. (1986). The physiology of wandering behaviour in Manduca sexta. IV. Hormonal induction of wandering behaviour from the isolated nervous system. *J. Exp. Biol.* **121**, 133-151. doi:10.1242/jeb.121.1.133

González, A., Hall, M. N., Lin, S. C. and Hardie, D. G. (2020). AMPK and TOR: The Yin and Yang of Cellular Nutrient Sensing and Growth Control. *Cell Metab.* **31**, 472-492. doi:10.1016/j.cmet.2020.01.015

Grueber, W. B., Ye, B., Moore, A. W., Jan, L. Y. and Jan, Y. N. (2003). Dendrites of distinct classes of Drosophila sensory neurons show different capacities for homotypic repulsion. *Curr. Biol.* **13**, 618-626. doi:10.1016/S0960-9822(03)00207-0

Gwinn, D. M., Shackelford, D. B., Egan, D. F., Mihaylova, M. M., Mery, A., Vasquez, D. S., Turk, B. E. and Shaw, R. J. (2008). AMPK phosphorylation of raptor mediates a metabolic checkpoint. *Mol. Cell* **30**, 214-226. doi:10.1016/j.molcel.2008.03.003

Hannus, M., Feiguin, F., Heisenberg, C. P. and Eaton, S. (2002). Planar cell polarization requires Widerborst, a B′ regulatory subunit of protein phosphatase 2A. *Development* **129**, 3493-3503. doi:10.1242/dev.129.14.3493

Hardie, D. G., Ross, F. A. and Hawley, S. A. (2012). AMPK: a nutrient and energy sensor that maintains energy homeostasis. *Nat. Rev. Mol. Cell Biol.* **13**, 251-262. doi:10.1038/nrm3311

Herzmann, S., Götzelmann, I., Reekers, L. F. and Rumpf, S. (2018). Spatial regulation of microtubule disruption during dendrite pruning in Drosophila. *Development* **145**, dev156950. doi:10.1242/dev.156950

Hochmuth, C. E., Biteau, B., Bohmann, D. and Jasper, H. (2011). Redox regulation by Keap1 and Nrf2 controls intestinal stem cell proliferation in Drosophila. *Cell Stem Cell* **8**, 188-199. doi:10.1016/j.stem.2010.12.006

Hung, R.-J., Yazdani, U., Yoon, J., Wu, H., Yang, T., Gupta, N., Huang, Z., van Berkel, W. J. H. and Terman, J. R. (2010). Mical links semaphorins to F-actin disassembly. *Nature* **463**, 823-827. doi:10.1038/nature08724

Joo, M. S., Kim, W. D., Lee, K. Y., Kim, J. H., Koo, J. H. and Kim, S. G. (2016). AMPK Facilitates nuclear accumulation of Nrf2 by phosphorylating at serine 550. *Mol. Cell. Biol.* **36**, 1931-1942. doi:10.1128/MCB.00118-16

Karim, F. D. and Thummel, C. S. (1992). Temporal coordination of regulatory gene expression by the steroid hormone ecdysone. *EMBO J.* **11**, 4083-4093. doi:10.1002/j.1460-2075.1992.tb05501.x

Kim, K.-Y., Baek, A., Hwang, J.-E., Choi, Y. A., Jeong, J., Lee, M.-S., Cho, D. H., Lim, J.-S., Kim, K. I. and Yang, Y. (2009). Adiponectin-activated AMPK stimulates dephosphorylation of AKT through protein phosphatase 2A activation. *Cancer Res.* **69**, 4018-4026. doi:10.1158/0008-5472.CAN-08-2641

Kirilly, D., Gu, Y., Huang, Y., Wu, Z., Bashirullah, A., Low, B. C., Kolodkin, A. L., Wang, H. and Yu, F. (2009). A genetic pathway composed of Sox14 and Mical governs severing of dendrites during pruning. *Nat. Neurosci.* **12**, 1497-1505. doi:10.1038/nn.2415

Kirilly, D., Wong, J. J., Lim, E. K., Wang, Y., Zhang, H., Wang, C., Liao, Q., Wang, H., Liou, Y.-C. and Yu, F. (2011). Intrinsic epigenetic factors cooperate

with the steroid hormone ecdysone to govern dendrite pruning in Drosophila. *Neuron* **72**, 86-100. doi:10.1016/j.neuron.2011.08.003

Kuo, C. T., Jan, L. Y. and Jan, Y. N. (2005). Dendrite-specific remodeling of Drosophila sensory neurons requires matrix metalloproteases, ubiquitin-proteasome, and ecdysone signaling. *Proc. Natl. Acad. Sci. U.S.A.* **102**, 15230-15235. doi:10.1073/pnas.0507393102

Kuo, C. T., Zhu, S., Younger, S., Jan, L. Y. and Jan, Y. N. (2006). Identification of E2/E3 ubiquitinating enzymes and caspase activity regulating Drosophila sensory neuron dendrite pruning. *Neuron* **51**, 283-290. doi:10.1016/j.neuron.2006.07.014

Lee, T., Marticke, S., Sung, C., Robinow, S. and Luo, L. (2000). Cell-autonomous requirement of the USP/EcR-B ecdysone receptor for mushroom body neuronal remodeling in Drosophila. *Neuron* **28**, 807-818. doi:10.1016/S0896-6273(00)00155-0

Lee, J. H., Koh, H., Kim, M., Kim, Y., Lee, S. Y., Karess, R. E., Lee, S.-H., Shong, M., Kim, J.-M., Kim, J. et al. (2007). Energy-dependent regulation of cell structure by AMP-activated protein kinase. *Nature* **447**, 1017-1020. doi:10.1038/nature05828

Loncle, N. and Williams, D. W. (2012). An interaction screen identifies headcase as a regulator of large-scale pruning. *J. Neurosci.* **32**, 17086-17096. doi:10.1523/JNEUROSCI.1391-12.2012

Luo, L. and O'Leary, D. D. (2005). Axon retraction and degeneration in development and disease. *Annu. Rev. Neurosci.* **28**, 127-156. doi:10.1146/annurev.neuro.28.061604.135632

Marchetti, G. and Tavosanis, G. (2017). Steroid hormone ecdysone signaling specifies mushroom body neuron sequential fate via chinmo. *Curr. Biol.* **27**, 3017-3024. doi:10.1016/j.cub.2017.08.037

Marzano, M., Herzmann, S., Elsbroek, L., Sanal, N., Tarbashevich, K., Raz, E., Krahn, M. P. and Rumpf, S. (2021). AMPK adapts metabolism to developmental energy requirement during dendrite pruning in Drosophila. *Cell reports* **37**, 110024. doi:10.1016/j.celrep.2021.110024

Matsubara, D., Horiuchi, S.-Y., Shimono, K., Usui, T. and Uemura, T. (2011). The seven-pass transmembrane cadherin Flamingo controls dendritic self-avoidance via its binding to a LIM domain protein, Espinas, in Drosophila sensory neurons. *Genes Dev.* **25**, 1982-1996. doi:10.1101/gad.16531611

Nakano, A., Kato, H., Watanabe, T., Min, K.-D., Yamazaki, S., Asano, Y., Seguchi, O., Higo, S., Shintani, Y., Asanuma, H. et al. (2010). AMPK controls the speed of microtubule polymerization and directional cell migration through CLIP-170 phosphorylation. *Nat. Cell Biol.* **12**, 583-590. doi:10.1038/ncb2060

Ng, C.-H., Guan, M. S. H., Koh, C., Ouyang, X., Yu, F., Tan, E.-K., O'Neill, S. P., Zhang, X., Chung, J. and Lim, K.-L. (2012). AMP kinase activation mitigates dopaminergic dysfunction and mitochondrial abnormalities in Drosophila models of Parkinson's disease. *J. Neurosci.* **32**, 14311-14317. doi:10.1523/JNEUROSCI.0499-12.2012

Riccomagno, M. M. and Kolodkin, A. L. (2015). Sculpting neural circuits by axon and dendrite pruning. *Annu. Rev. Cell Dev. Biol.* **31**, 779-805. doi:10.1146/annurev-cellbio-100913-013038

Rode, S., Ohm, H., Anhäuser, L., Wagner, M., Rosing, M., Deng, X., Sin, O., Leidel, S. A., Storkebaum, E., Rentmeister, A. et al. (2018). Differential requirement for translation initiation factor pathways during ecdysone-dependent neuronal remodeling in Drosophila. *Cell Rep.* **24**, 2287-2299. doi:10.1016/j.celrep.2018.07.074

Rui, M., Ng, K. S., Tang, Q., Bu, S. and Yu, F. (2020). Protein phosphatase PP2A regulates microtubule orientation and dendrite pruning in Drosophila. *EMBO Rep.* **21**, e48843. doi:10.15252/embr.201948843

Rumpf, S., Lee, S. B., Jan, L. Y. and Jan, Y. N. (2011). Neuronal remodeling and apoptosis require VCP-dependent degradation of the apoptosis inhibitor DIAP1. *Development* **138**, 1153-1160. doi:10.1242/dev.062703

Schuldiner, O. and Yaron, A. (2015). Mechanisms of developmental neurite pruning. *Cell. Mol. Life Sci.* **72**, 101-119. doi:10.1007/s00018-014-1729-6

Schuldiner, O., Berdnik, D., Levy, J. M., Wu, J. S., Luginbuhl, D., Gontang, A. C. and Luo, L. (2008). piggyBac-based mosaic screen identifies a postmitotic function for cohesin in regulating developmental axon pruning. *Dev. Cell* **14**, 227-238. doi:10.1016/j.devcel.2007.11.001

Sellgren, C. M., Gracias, J., Watmuff, B., Biag, J. D., Thanos, J. M., Whittredge, P. B., Fu, T., Worringer, K., Brown, H. E., Wang, J. et al. (2019). Increased synapse elimination by microglia in schizophrenia patient-derived models of synaptic pruning. *Nat. Neurosci.* **22**, 374-385. doi:10.1038/s41593-018-0334-7

Shimono, K., Fujimoto, A., Tsuyama, T., Yamamoto-Kochi, M., Sato, M., Hattori, Y., Sugimura, K., Usui, T., Kimura, K. and Uemura, T. (2009). Multidendritic sensory neurons in the adult Drosophila abdomen: origins, dendritic morphology, and segment- and age-dependent programmed cell death. *Neural Dev.* **4**, 37. doi:10.1186/1749-8104-4-37

Swick, L. L., Kazgan, N., Onyenwoke, R. U. and Brenman, J. E. (2013). Isolation of AMP-activated protein kinase (AMPK) alleles required for neuronal maintenance in Drosophila melanogaster. *Biol. Open* **2**, 1321-1323. doi:10.1242/bio.20136775

Sykiotis, G. P. and Bohmann, D. (2008). Keap1/Nrf2 signaling regulates oxidative stress tolerance and lifespan in Drosophila. *Dev. Cell* **14**, 76-85. doi:10.1016/j.devcel.2007.12.002

Tang, G., Gudsnuk, K., Kuo, S.-H., Cotrina, M. L., Rosoklija, G., Sosunov, A., Sonders, M. S., Kanter, E., Castagna, C., Yamamoto, A. et al. (2014). Loss of mTOR-dependent macroautophagy causes autistic-like synaptic pruning deficits. *Neuron* **83**, 1131-1143. doi:10.1016/j.neuron.2014.07.040

Tang, Q., Rui, M., Bu, S., Wang, Y., Chew, L. Y. and Yu, F. (2020). A microtubule polymerase is required for microtubule orientation and dendrite pruning in Drosophila. *EMBO J.* **39**, e103549. doi:10.15252/embj.2019103549

Teleman, A. A., Chen, Y.-W. and Cohen, S. M. (2005). 4E-BP functions as a metabolic brake used under stress conditions but not during normal growth. *Genes Dev.* **19**, 1844-1848. doi:10.1101/gad.341505

Terman, J. R., Mao, T., Pasterkamp, R. J., Yu, H.-H. and Kolodkin, A. L. (2002). MICALs, a family of conserved flavoprotein oxidoreductases, function in plexin-mediated axonal repulsion. *Cell* **109**, 887-900. doi:10.1016/S0092-8674(02)00794-8

Thummel, C. S. (1996). Flies on steroids–Drosophila metamorphosis and the mechanisms of steroid hormone action. *Trends Genet.* **12**, 306-310. doi:10.1016/0168-9525(96)10032-9

Trefts, E. and Shaw, R. J. (2021). AMPK: restoring metabolic homeostasis over space and time. *Mol. Cell* **81**, 3677-3690. doi:10.1016/j.molcel.2021.08.015

Truman, J. W. (1990). Metamorphosis of the central nervous system of Drosophila. *J. Neurobiol.* **21**, 1072-1084. doi:10.1002/neu.480210711

Tullet, J. M., Hertweck, M., An, J. H., Baker, J., Hwang, J. Y., Liu, S., Oliveira, R. P., Baumeister, R. and Blackwell, T. K. (2008). Direct inhibition of the longevity-promoting factor SKN-1 by insulin-like signaling in C. elegans. *Cell* **132**, 1025-1038. doi:10.1016/j.cell.2008.01.030

Ulgherait, M., Rana, A., Rera, M., Graniel, J. and Walker, D. W. (2014). AMPK modulates tissue and organismal aging in a non-cell-autonomous manner. *Cell Rep.* **8**, 1767-1780. doi:10.1016/j.celrep.2014.08.006

Wang, S., Liu, S., Liu, H., Wang, J., Zhou, S., Jiang, R.-J., Bendena, W. G. and Li, S. (2010). 20-hydroxyecdysone reduces insect food consumption resulting in fat body lipolysis during molting and pupation. *J. Mol. Cell Biol.* **2**, 128-138. doi:10.1093/jmcb/mjq006

Wang, Y., Rui, M., Tang, Q., Bu, S. and Yu, F. (2019). Patronin governs minus-end-out orientation of dendritic microtubules to promote dendrite pruning in Drosophila. *eLife* **8**, e39964. doi:10.7554/eLife.39964.041

Williams, D. W. and Truman, J. W. (2005). Cellular mechanisms of dendrite pruning in Drosophila: insights from in vivo time-lapse of remodeling dendritic arborizing sensory neurons. *Development* **132**, 3631-3642. doi:10.1242/dev.01928

Witte, H., Neukirchen, D. and Bradke, F. (2008). Microtubule stabilization specifies initial neuronal polarization. *J. Cell Biol.* **180**, 619-632. doi:10.1083/jcb.200707042

Wolterhoff, N., Gigengack, U. and Rumpf, S. (2020). PP2A phosphatase is required for dendrite pruning via actin regulation in Drosophila. *EMBO Rep.* **21**, e48870. doi:10.15252/embr.201948870

Wong, J. J., Li, S., Lim, E. K., Wang, Y., Wang, C., Zhang, H., Kirilly, D., Wu, C., Liou, Y. C., Wang, H. et al. (2013). A Cullin1-based SCF E3 ubiquitin ligase targets the InR/PI3K/TOR pathway to regulate neuronal pruning. *PLoS Biol.* **11**, e1001657. doi:10.1371/journal.pbio.1001657

Yashirogi, S., Nagao, T., Nishida, Y., Takahashi, Y., Qaqorh, T., Yazawa, I., Katayama, T., Kioka, H., Matsui, T. S., Saito, S. et al. (2021). AMPK regulates cell shape of cardiomyocytes by modulating turnover of microtubules through CLIP-170. *EMBO Rep.* **22**, e50949. doi:10.15252/embr.202050949

Yu, F. and Schuldiner, O. (2014). Axon and dendrite pruning in Drosophila. *Curr. Opin. Neurobiol.* **27**, 192-198. doi:10.1016/j.conb.2014.04.005

Yuan, D., Zhou, S., Liu, S., Li, K., Zhao, H., Long, S., Liu, H., Xie, Y., Su, Y., Yu, F. et al. (2020). The AMPK-PP2A axis in insect fat body is activated by 20-hydroxyecdysone to antagonize insulin/IGF signaling and restrict growth rate. *Proc. Natl. Acad. Sci. U.S.A.* **117**, 9292-9301. doi:10.1073/pnas.2000963117

Zhang, H., Wang, Y., Wong, J. J. L., Lim, K.-L., Liou, Y.- C., Wang, H. and Yu, F. (2014). Endocytic pathways downregulate the L1-type cell adhesion molecule neuroglian to promote dendrite pruning in Drosophila. *Dev. Cell* **30**, 463-478. doi:10.1016/j.devcel.2014.06.014

Zheng, X., Wang, J., Haerry, T. E., Wu, A. Y., Martin, J., O'Connor, M. B., Lee, C. H. and Lee, T. (2003). TGF-beta signaling activates steroid hormone receptor expression during neuronal remodeling in the Drosophila brain. *Cell* **112**, 303-315. doi:10.1016/S0092-8674(03)00072-2

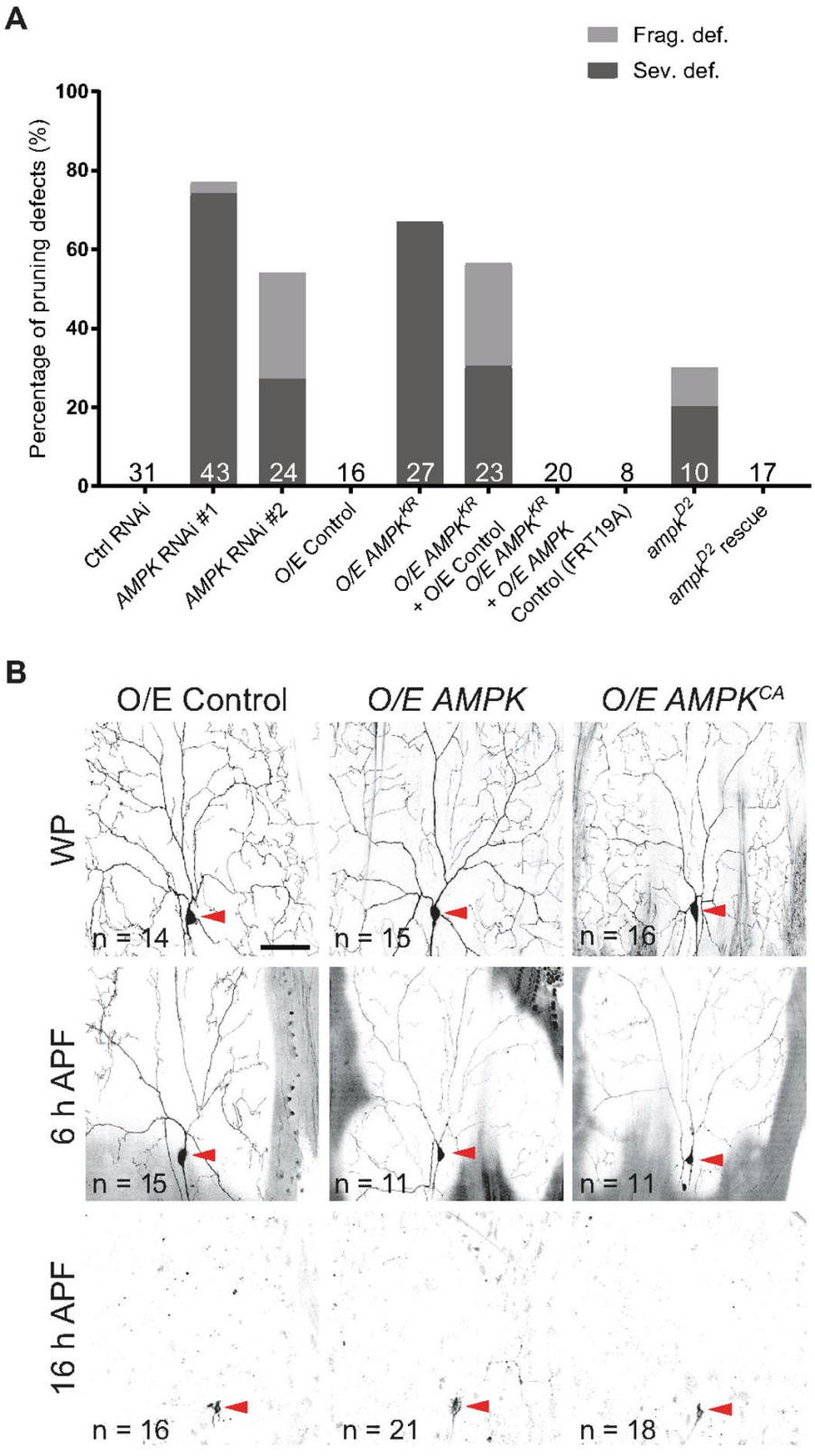

Development • Supplementary information

Fig. S1. Overexpression of AMPK or AMPK^{CA} does not affect dendrite pruning at 6 h and 16 h APF.

A) Percentages of ddaC neurons showing severing or fragmentation defects at 16 h APF. (B) Dendrites of control, AMPK- or AMPK^{CA}-overexpressing ddaC neurons at WP, 6 h APF and 16 h APF stages. Red arrowheads point to the somata of ddaC neurons. The number of neurons (n) examined in each group is shown on the bars. The scale bar in (B) represents 50 μm.

Development • Supplementary information

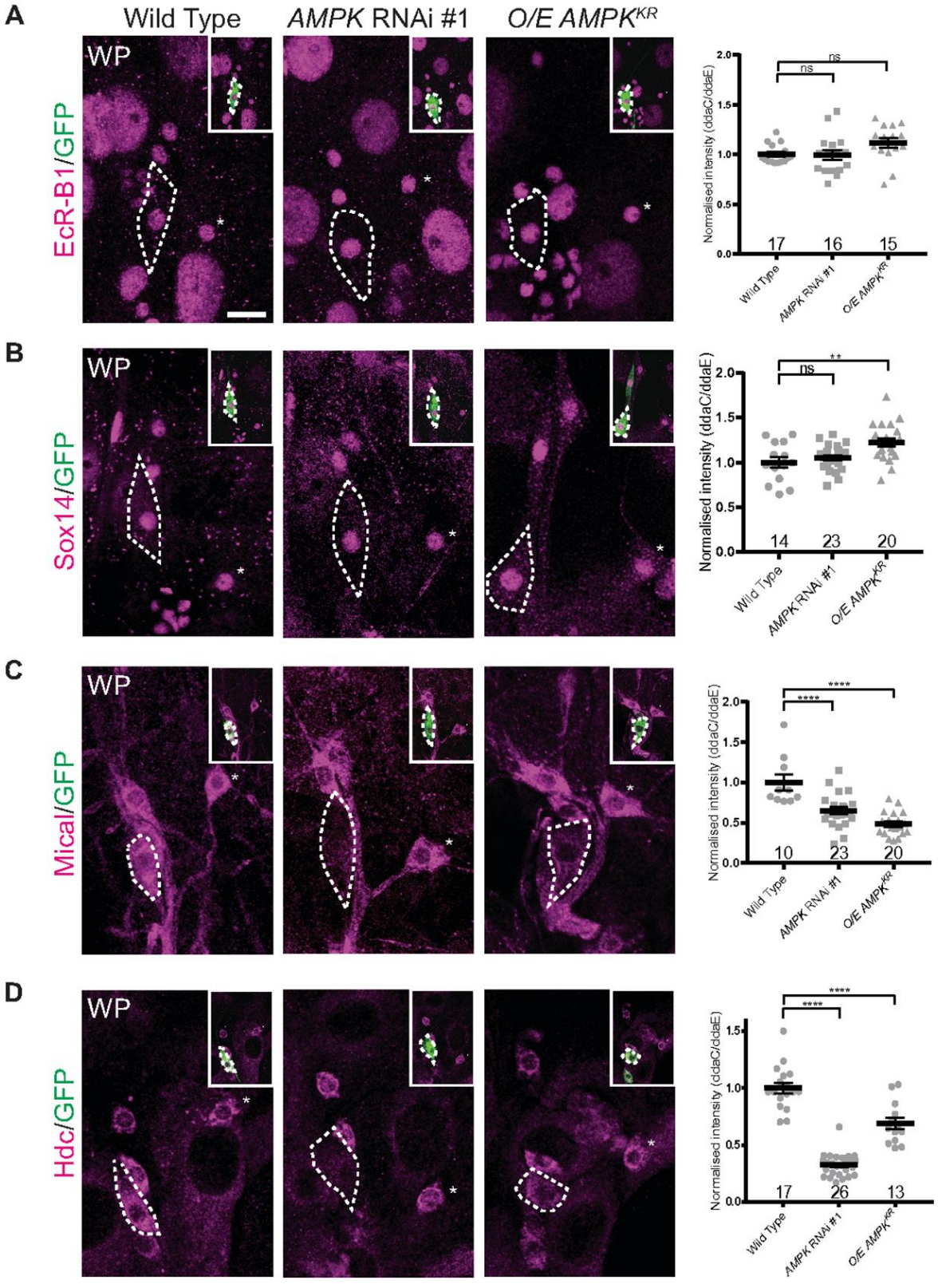

Development • Supplementary information

Fig. S2. AMPK is required for the expression of Mical/Hdc.

(A-D) Expression of EcR-B1 (A), Sox14 (B), Mical (C) and Hdc (D) in wild-type, *AMPK* RNAi #1 and $AMPK^{KR}$ ddaC neurons at WP stage. ddaC somata are marked by dashed lines. Quantitative analyses of normalized EcR-B1, Sox14, Mical and Hdc fluorescence are shown in the rightest panels. Error bars represent ± SEM. One-way ANOVA with Bonferroni test was applied to determine significance for multiple-group comparison. ns, not significant, **p<0.01, ****p<0.0001. The number of neurons (n) examined in each group is shown on the bars. The scale bar in (A) represents 10 μm.

Development • Supplementary information

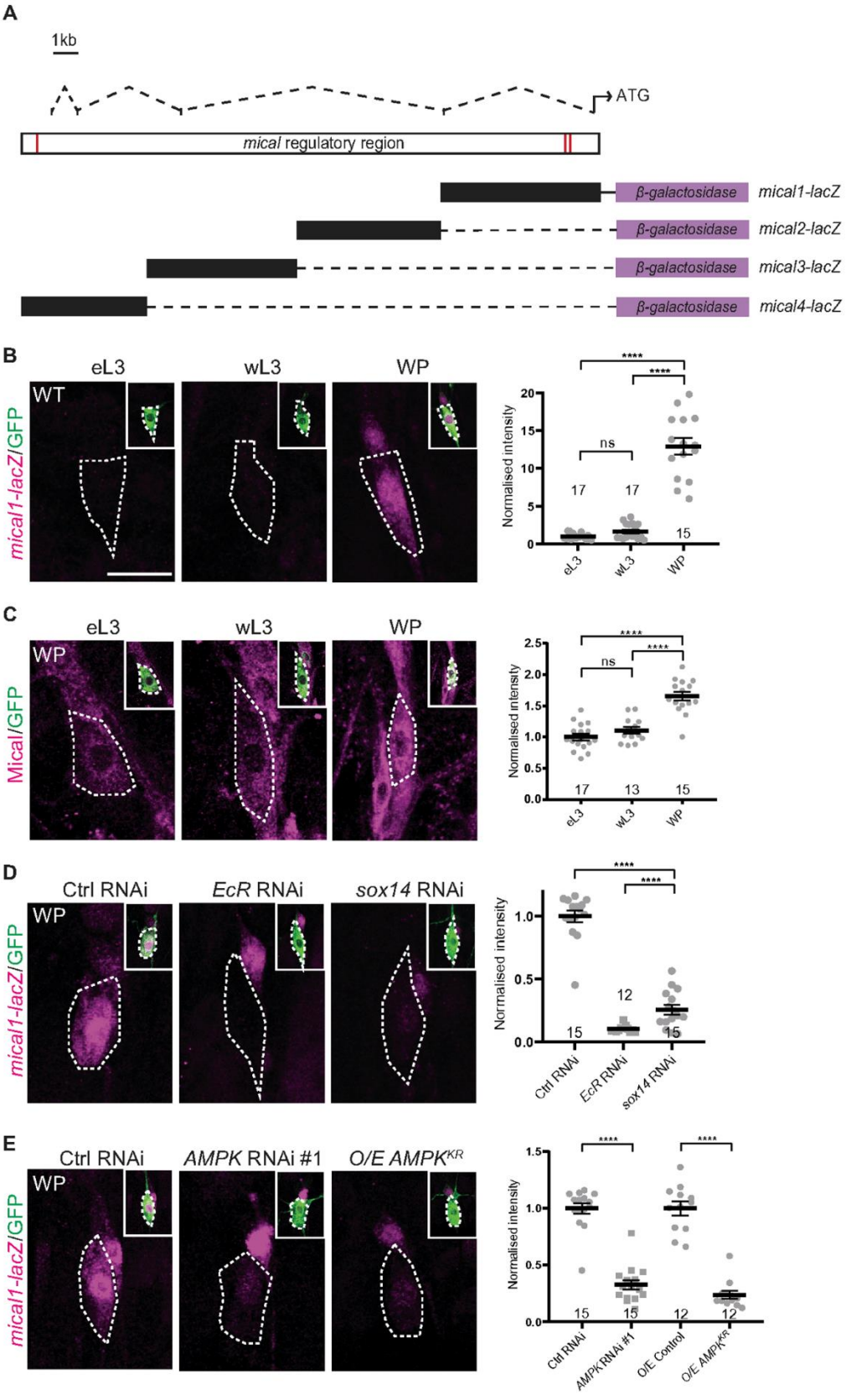

Development • Supplementary information

Fig. S3. AMPK induces Mical expression.

(A) The regulatory region of *mical* gene. Four *lacZ* reporter lines under the control of *mical* enhancers were generated. Red lines indicate three putative ecdysone-response elements. (B-C) Expression of *mical1-lacZ* (B) and Mical (C) in wild-type ddaC neurons at eL3, wL3 and WP stages. (D-E) Expression of *mical1-lacZ* in control RNAi, *EcR* RNAi and *sox14* RNAi ddaC neurons (D), control RNAi, *AMPK* RNAi #1 and $AMPK^{KR}$-overexpressing neurons (E) at WP stage. ddaC somata are marked by dashed lines. Quantitative analyses of normalized *mical1-lacZ* and Mical fluorescence are shown in the rightest panels. Error bars represent ± SEM. Two-tailed Student's T-test was used to determine statistical significance for pairwise comparison, whereas one-way ANOVA with Bonferroni test was applied to determine significance for multiple-group comparison. ns, not significant, ****$p<0.0001$. The number of neurons (n) examined in each group is shown on the bars. The scale bar in (B) represents 10 μm.

Development • Supplementary information

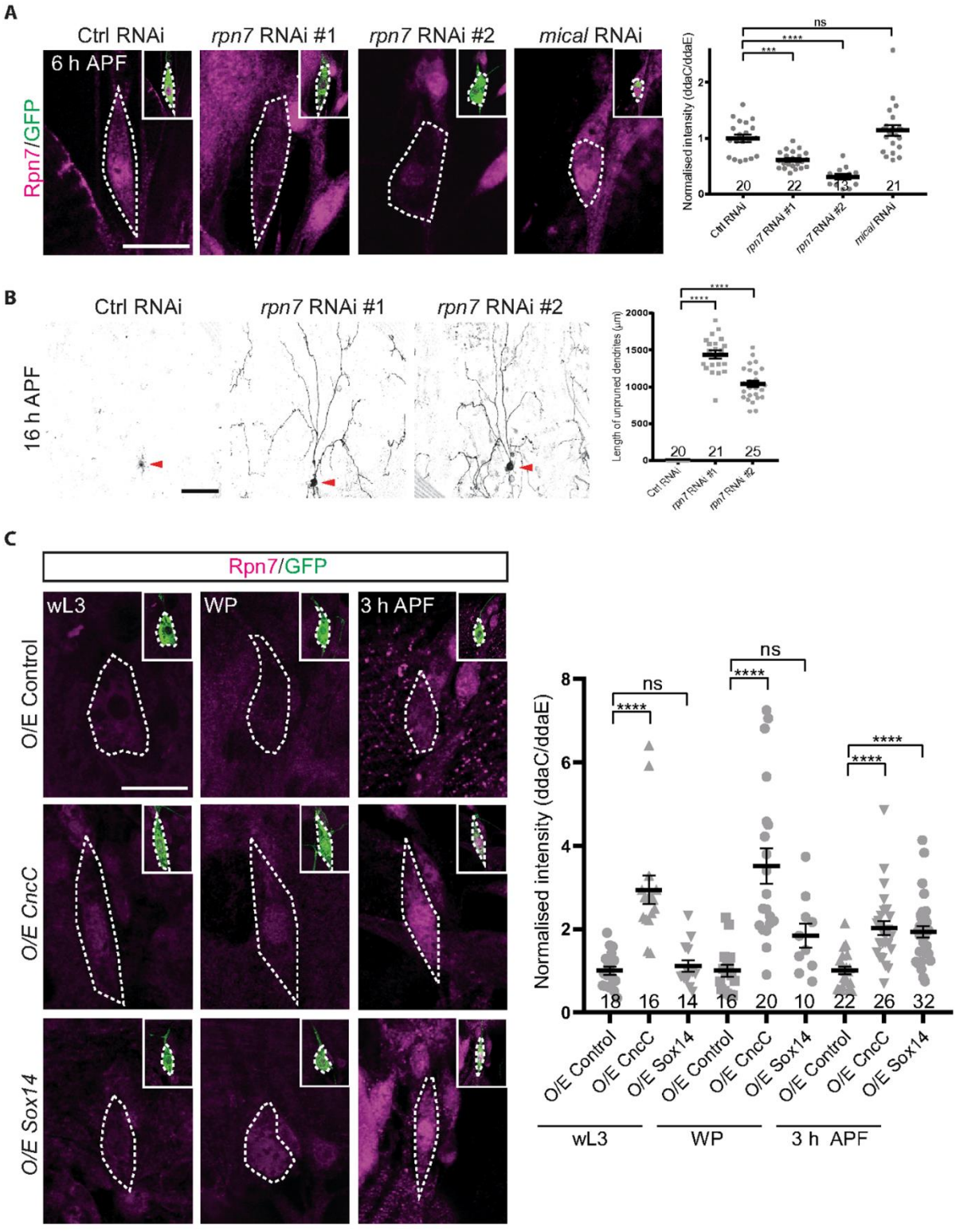

Development • Supplementary information

Fig. S4. Overexpression of CncC or Sox14 leads to elevated Rpn7 expression.

(A, C) Expression of Rpn7 in control RNAi, *rpn7* RNAi #1/#2, and *mical* RNAi (A), control, CncC-overexpressing and Sox14-overexpressing ddaC neurons at 6 h APF (A) or wL3, WP and 3 h APF stages (C). ddaC somata are marked by dashed lines. Quantitative analyses of normalized Rpn7 fluorescence are shown in the rightest panels. (B) Dendrites of control RNAi, *rpn7* RNAi #1, or #2 at 16 h APF stages. Quantitative analysis of unpruned dendrite length at 16 h APF. Red arrowheads point to the somata of ddaC neurons. Error bars represent ± SEM. One-way ANOVA with Bonferroni test was applied to determine significance for multiple-group comparison. ns, not significant, ***p< 0.001, ****p<0.0001. The number of neurons (n) examined in each group is shown on the bars. The scale bars in (A, C) and (B) represent 10 μm and 50 μm, respectively.

Development • Supplementary information

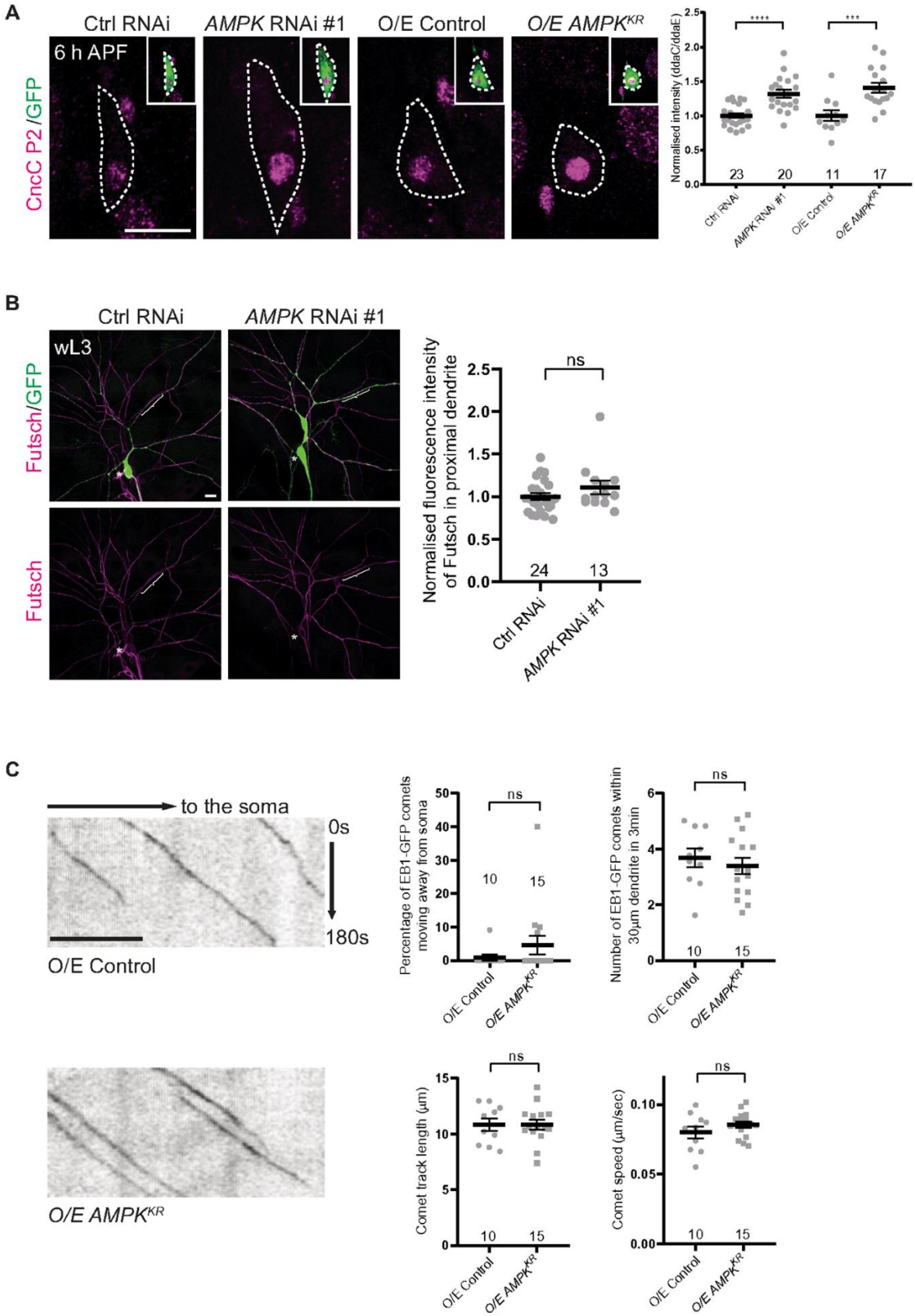

Development • Supplementary information

Fig. S5. AMPK does not affect microtubule mass or polarity in ddaC dendrites.

(A) Expression of CncC in control RNAi, *AMPK* RNAi #1, control and $AMPK^{KR}$-overexpressing ddaC neurons at 6 h APF. ddaC somata are marked by dashed lines. (B) Expression of Futsch in control RNAi and *AMPK* RNAi #1 ddaC neurons at wL3 stage. Quantitative analysis of normalized Futsch fluorescence in proximal dendrites is shown in the rightest panel. The ddaC somata are labelled by asterisks and the dendrites by brackets. (C) Representative kymographs depicting the movement patterns of EB1 comets in the proximal dendrites of control and $AMPK^{KR}$-overexpressing ddaC neurons at 96 h AEL. Quantitative analyses of the percentages of anterograde EB1 comets in each neuron, the average numbers of EB1-GFP comets within 30 μm dendrite in 3 min, the average comet track length, and the average comet speed are shown in the right panels. Error bars represent ± SEM. ns, not significant. Two-tailed Student's T-test was used to determine statistical significance for pairwise comparison. ns, not significant, ***$p< 0.001$, ****$p<0.0001$. The number of neurons (n) examined in each group is shown on the bars. The scale bars in (A-C) represent 10 μm.

Development • Supplementary information

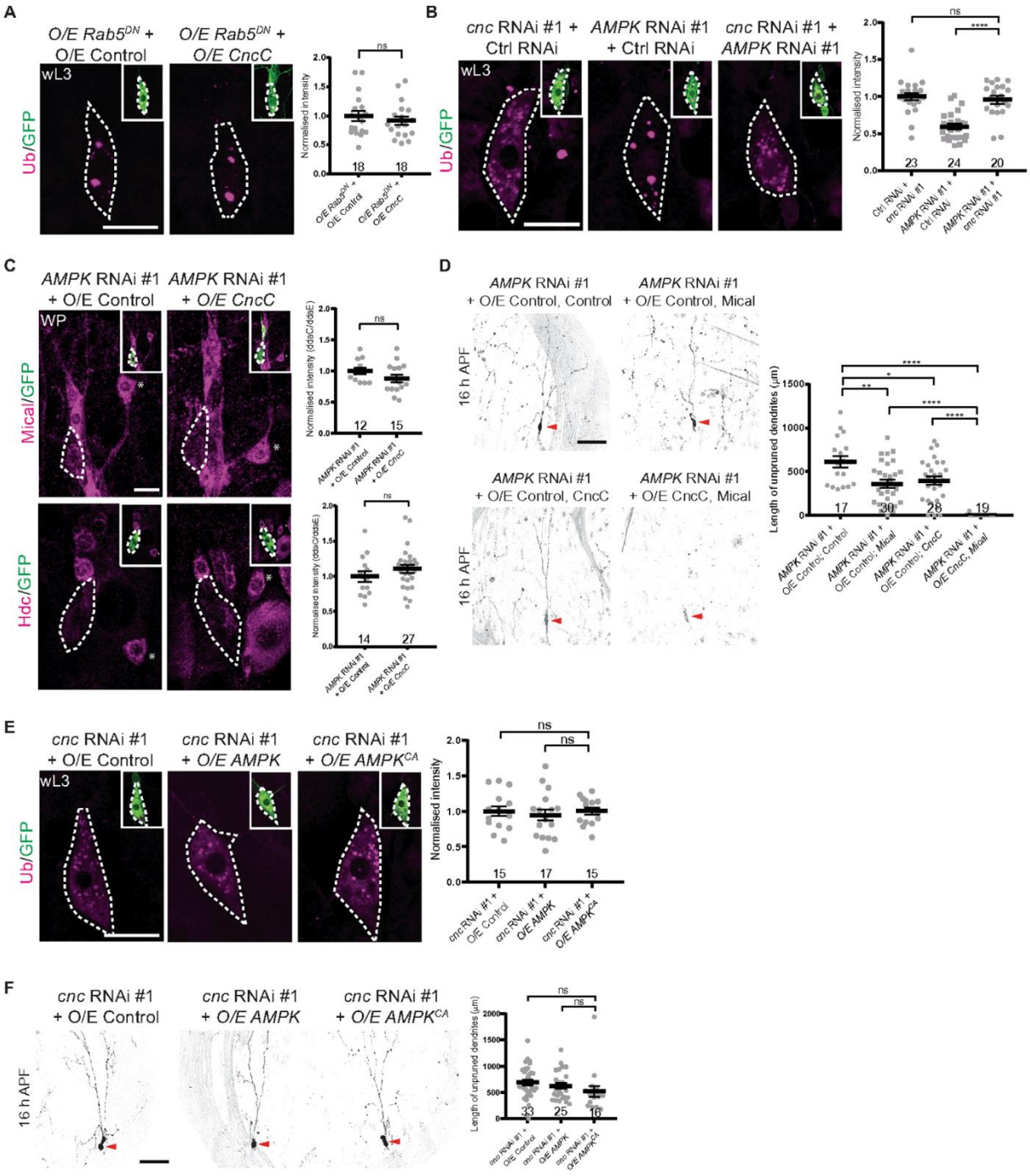

Development • Supplementary information

Fig. S6. Overexpression of AMPK^{CA} does not rescue the *cncC* RNAi defects in terms of ubiquitinated protein aggregation and dendrite pruning.

(A-B) Levels of ubiquitinated protein aggregates in *Rab5^{DN}* neurons co-overexpressing control or CncC (A), *cncC* RNAi #1 neurons overexpressing control RNAi or *AMPK* RNAi as well as *AMPK* RNAi #1 overexpressing control RNAi at wL3 stage (B). (C) Expression of Mical and Hdc in *AMPK* RNAi #1 neurons overexpressing control or CncC at WP stage. (D) Dendrites of *AMPK* RNAi #1 neurons overexpressing control + control, control + Mical, control + CncC, and CncC + Mical at 16 h APF. (E) Levels of ubiquitinated protein aggregates in *cncC* RNAi #1 neurons overexpressing control, AMPK or AMPK^{CA} at wL3 stage. ddaC somata are marked by dashed lines. (F) Dendrites of *cncC* RNAi #1 neurons overexpressing control, AMPK or AMPK^{CA} at 16 h APF. Red arrowheads point to the somata of ddaC neurons. Quantitative analyses of normalized Mical, Hdc and ubiquitinated protein aggregates fluorescence are shown in the rightest panels (A-C, E). Quantitative analysis of unpruned dendrite length at 16 h APF are shown at the right panels (D, F). Error bars represent ± SEM. Two-tailed Student's T-test was used to determine statistical significance for pairwise comparison, whereas one-way ANOVA with Bonferroni test was applied to determine significance for multiple-group comparison. ns, not significant, *p<0.05, **p<0.01, ****p<0.0001. The number of neurons (n) examined in each group is shown on the bars. The scale bars in (A-C, E) and (D, F) represent 10 μm and 50 μm, respectively.

Development • Supplementary information

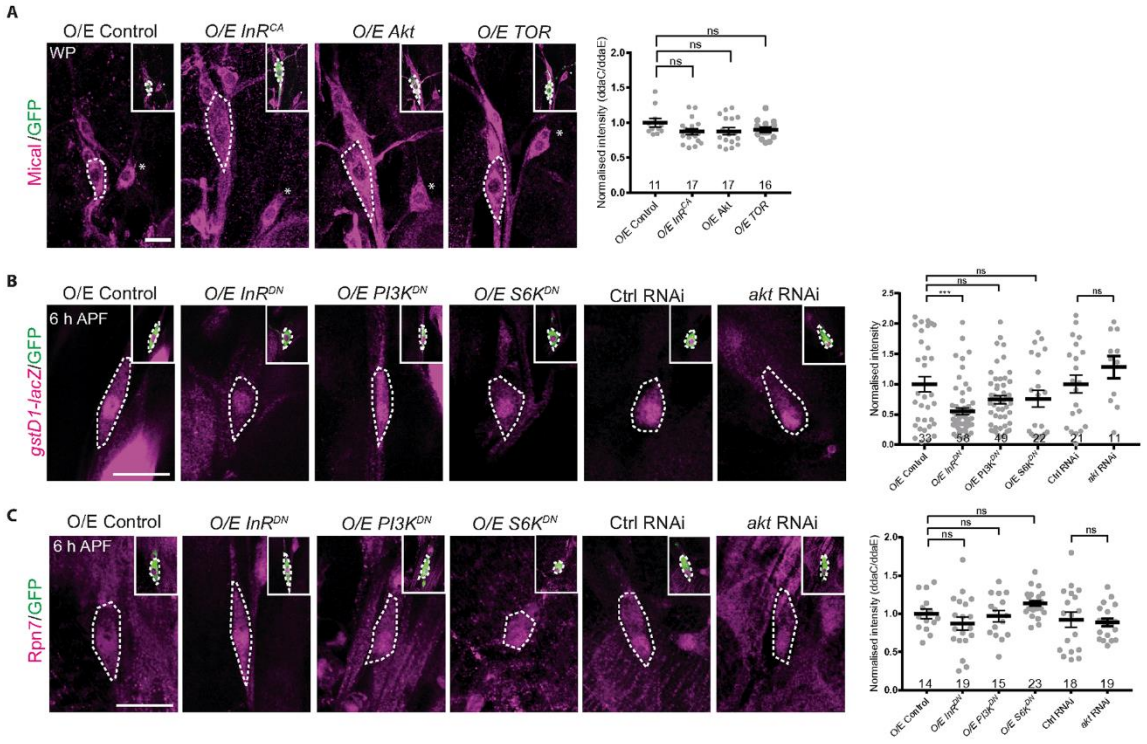

Fig. S7. Inhibition of insulin-TOR pathway is not sufficient for the activation of Nrf2-Keap1 pathway in ddaC neurons.

(A) Expression of Mical in InR^{CA}, Akt or TOR-overexpressing ddaC neurons at WP stage. (B) Expression of *gstD1-lacZ* in control, InR^{DN}-overexpressing, $PI3K^{DN}$-overexpressing, $S6K^{DN}$-overexpressing, control RNAi and *akt* RNAi ddaC neurons at 6 h APF. (C) Expression of Rpn7 in control, InR^{DN}-overexpressing, $PI3K^{DN}$-overexpressing, $S6K^{DN}$-overexpressing, control RNAi and *akt* RNAi ddaC neurons at 6 h APF. ddaC somata are marked by dashed lines. Quantitative analyses of normalized Mical, *gstD1-lacZ* and Rpn7 fluorescence are shown in the rightest panels (A-C). Error bars represent ± SEM. Two-tailed Student's T-test was used to determine statistical significance for pairwise comparison, whereas one-way ANOVA with Bonferroni test was applied to determine significance for multiple-group comparison. ns, not significant. The number of neurons (n) examined in each group is shown on the bars. The scale bars in (A-C) represent 10 μm.

Development • Supplementary information

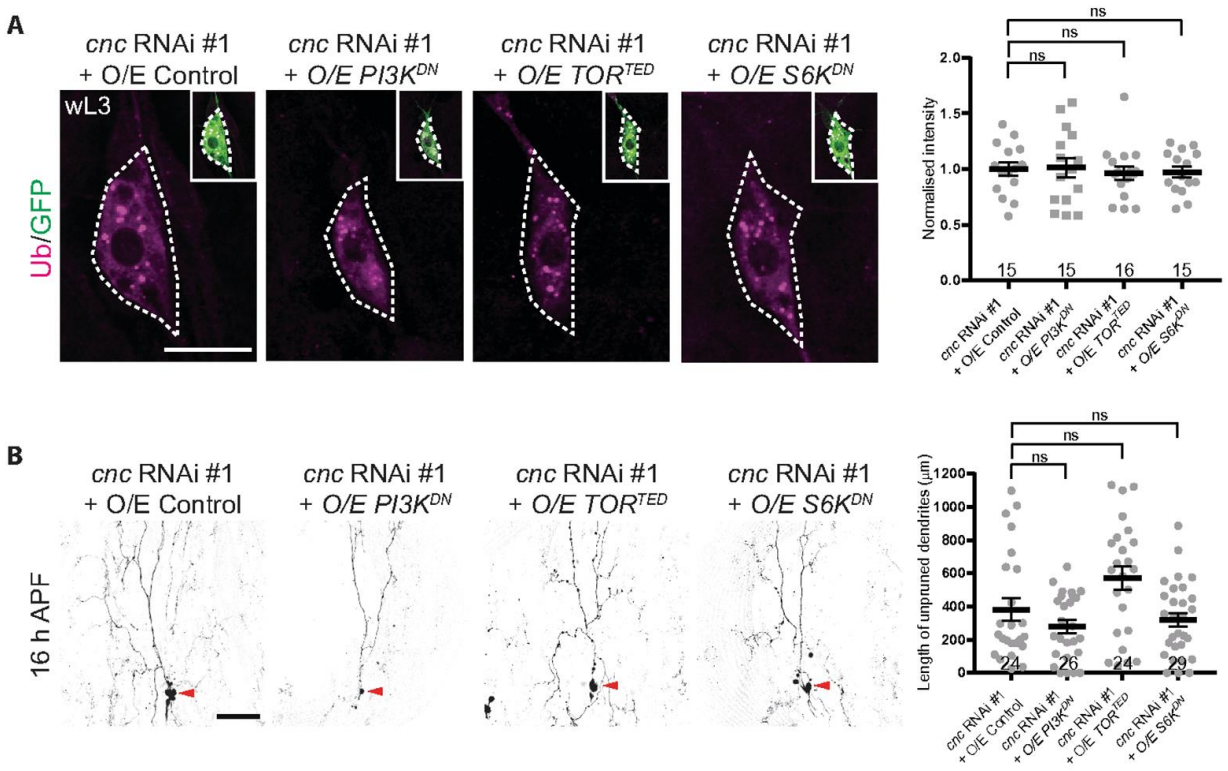

Fig. S8. The *cncC* RNAi defects are not rescued by attenuation of insulin-TOR pathway.

(A) Levels of ubiquitinated protein aggregates in *cncC* RNAi #1 ddaC neurons overexpressing control, PI3K^{DN}, TOR^{TED} or S6K^{DN}. ddaC somata are marked by dashed lines. (B) Dendrites of *cnc* RNAi #1 ddaC neurons overexpressing control, PI3K^{DN}, TOR^{TED} or S6K^{DN} at 16 h APF. Red arrowheads point to the somata of ddaC neurons. Quantitative analyses of normalized ubiquitinated protein aggregates fluorescence are shown in the rightest panels (A). Quantitative analysis of unpruned dendrite length at 16 h APF is shown in the rightest panel (B). Error bars represent ± SEM. One-way ANOVA with Bonferroni test was applied to determine significance for multiple-group comparison. ns, not significant. The number of neurons (n) examined in each group is shown on the bars. The scale bars in (A) and (B) represent 10 μm and 50 μm, respectively.

Development • Supplementary information

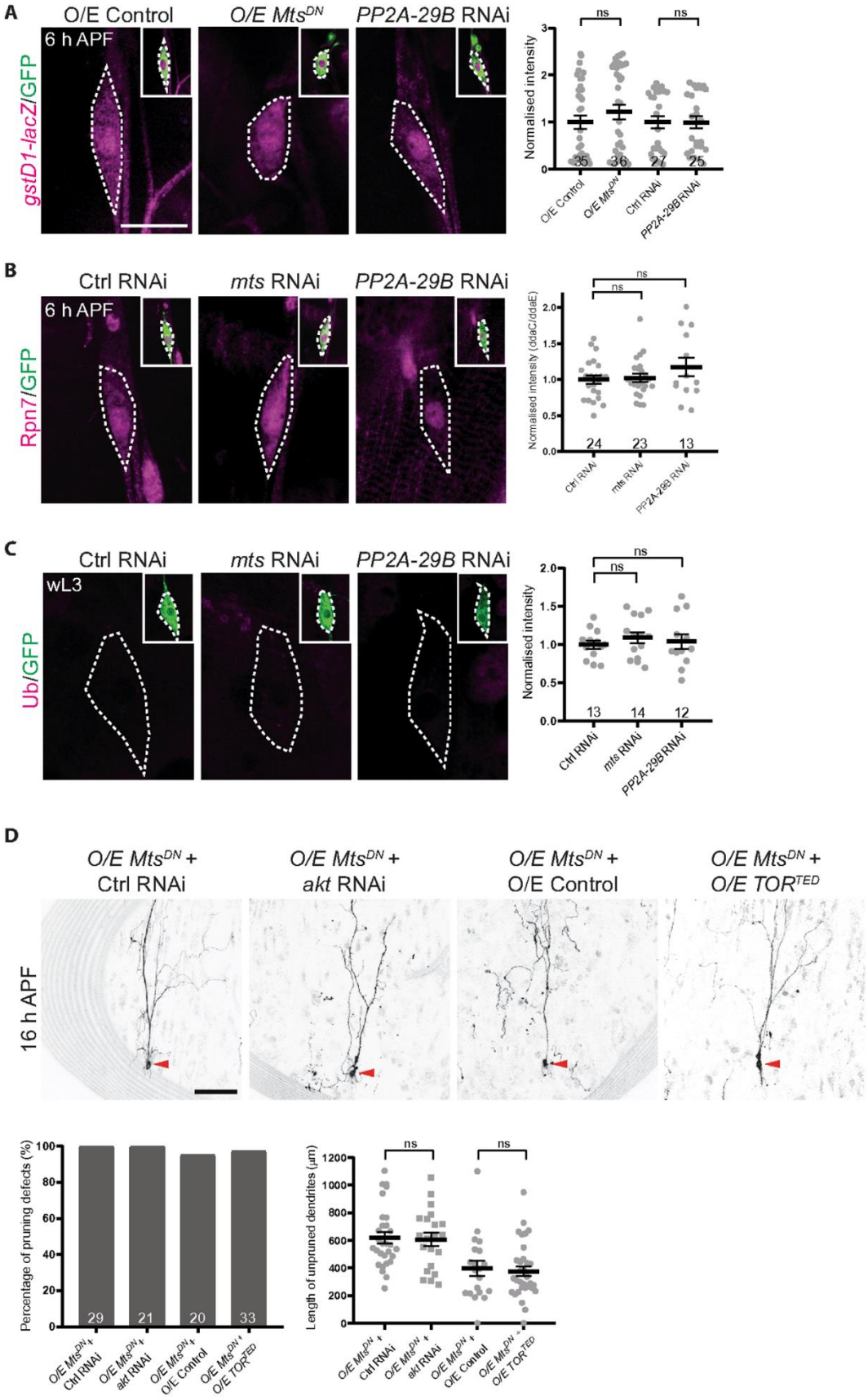

Development • Supplementary information

Fig. S9. PP2A is dispensable for activation of Nrf2-Keap1 pathway.

(A-C) Expression levels of *gstD1-lacZ* (A), Rpn7 (B) and ubiquitinated protein aggregates (C) in control, Mts^{DN} or *mts* RNAi, *PP2A-29B* RNAi ddaC neurons at 6 h APF (A-B) or wL3 (C) stage. ddaC somata are marked by dashed lines. (D) Dendrites of Mts^{DN} neurons expressing control RNAi, *akt* RNAi, control or TOR^{TED} at 16 h APF. Red arrowheads point to the somata of ddaC neurons. Quantitative analyses of normalized *gstD1-lacZ*, Rpn7 and ubiquitinated protein aggregates fluorescence are shown in the rightest panels (A-C). Quantitative analyses of percentage of pruning defects and unpruned dendrite length at 16 h APF are shown in the bottom panels (D). Error bars represent ± SEM. Two-tailed Student's T-test was used to determine statistical significance for pairwise comparison, whereas one-way ANOVA with Bonferroni test was applied to determine significance for multiple-group comparison. ns, not significant. The number of neurons (n) examined in each group is shown on the bars. The scale bars in (A) and (D) represent 10 μm and 50 μm, respectively.

Development • Supplementary information

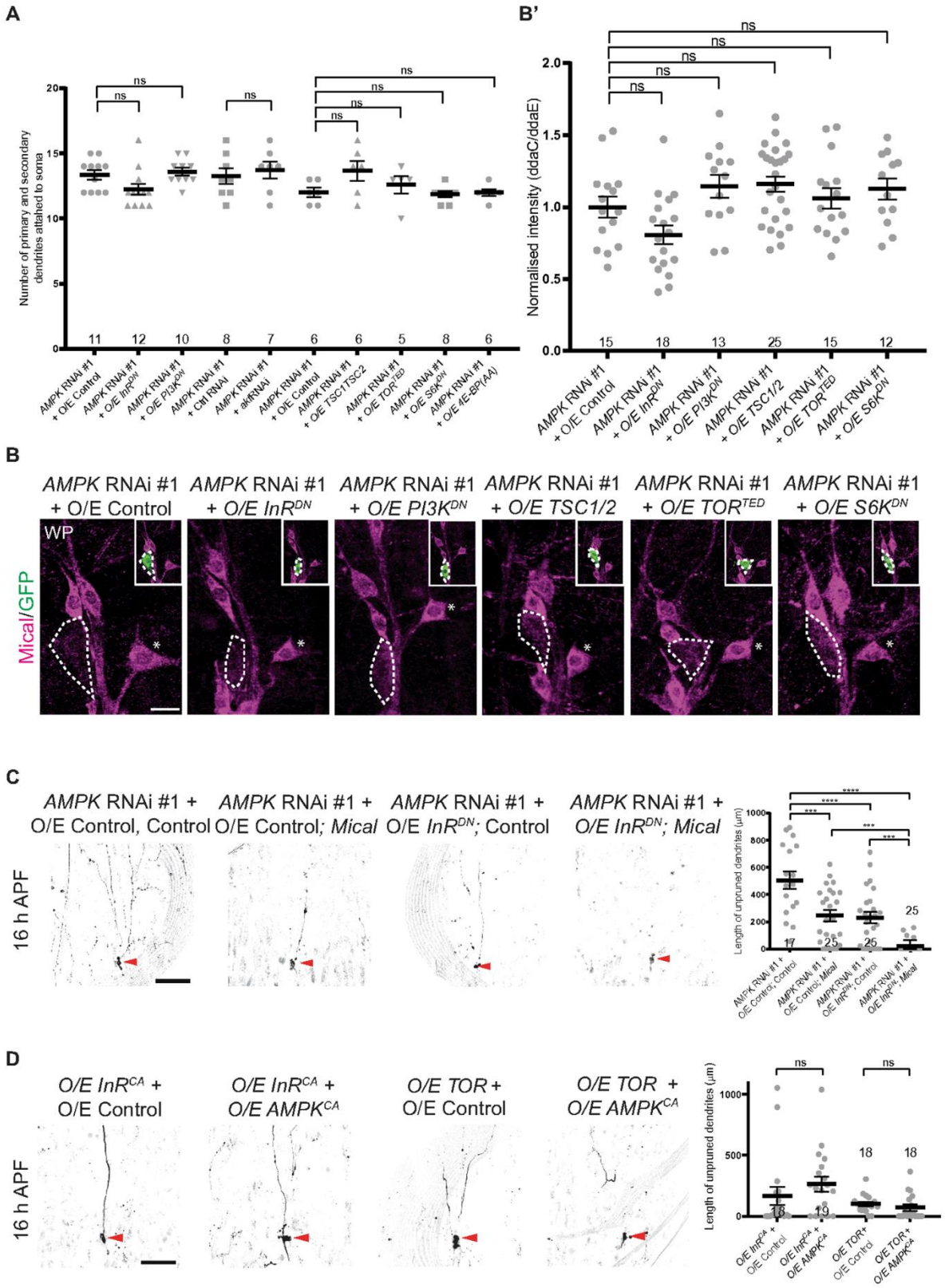

Development • Supplementary information

Fig. S10. Attenuation of insulin-TOR pathway does not restore Mical expression in *AMPK* RNAi #1 neurons.

(A) Quantitative analysis of the number of primary and secondary dendrites in ddaC neurons at WP stage. (B) Expression of Mical in *AMPK* RNAi #1 ddaC neurons expressing control, InR^{DN}, $PI3K^{DN}$, TSC1/2, TOR^{TED}, and $S6K^{DN}$ at WP stage. ddaC somata are marked by dashed lines. (C) Dendrites of *AMPK* RNAi #1 neurons overexpressing control + control, control + Mical, control + InR^{DN}, and Mical + InR^{DN} at 16 h APF. (D) Dendrites of control or $AMPK^{CA}$ neurons co-expressing InR^{CA} or TOR at 16 h APF. Red arrowheads point to the somata of ddaC neurons. Quantitative analyses of normalized Mical fluorescence are shown in the panel (B'). Quantitative analysis of unpruned dendrite length at 16 h APF are shown in the rightest panel (C-D). Error bars represent ± SEM. Two-tailed Student's T-test was used to determine statistical significance for pairwise comparison, whereas one-way ANOVA with Bonferroni test was applied to determine significance for multiple-group comparison. ns, not significant, ***$p<0.001$, ****$p<0.0001$. The number of neurons (n) examined in each group is shown on the bars. The scale bars in (B) and (C-D) represent 10 μm and 50 μm, respectively.

Development • Supplementary information

Supplementary Materials and Methods

Genotypes of fly strains

Figure 1: (B) *w*;* UAS-Control RNAi / UAS-Control RNAi; *ppk-Gal4, UAS-mCD8GFP, UAS-Dcr2 / ppk-Gal4, UAS-mCD8GFP, UAS-Dcr2.* **(C)** *w*; UAS-AMPK* RNAi #1 / *UAS-AMPK* RNAi #1; *ppk-Gal4, UAS-mCD8GFP, UAS-Dcr2 / ppk-Gal4, UAS-mCD8GFP, UAS-Dcr2*. **(D)** *w*; ppk-Gal4, UAS-mCD8GFP, UAS-Dcr2 / ppk-Gal4, UAS-mCD8GFP, UAS-Dcr2*; *UAS-AMPK* RNAi #2 / *UAS-AMPK* RNAi #2. **(E)** *w*; ppk-Gal4, UAS-mCD8GFP / ppk-Gal4, UAS-mCD8GFP; UAS-AMPK^{KR} / UAS-AMPK^{KR}*. **(F)** *w*; ppk-Gal4, UAS-mCD8GFP / ppk-Gal4, UAS-mCD8GFP; UAS-AMPK^{KR} / UAS-Mical^{NT}*. **(G)** *w*; ppk-Gal4, UAS-mCD8GFP / UAS-AMPK; UAS-AMPK^{KR} / ppk-Gal4, UAS-mCD8GFP*. **(H) Control (FRT19A):** *FRT19A / FRT19A, tubP-Gal80, hs-FLP, w*; ppk-Gal4, UAS-mCD8GFP, SOP-flp / +*. **ampk^{D2}:** *FRT19A, ampk^{D2} / FRT19A, tubP-Gal80, hs-FLP, w*; ppk-Gal4, UAS-mCD8GFP, SOP-flp / +*. **(I)** *FRT19A, ampk^{D2} / FRT19A, tubP-Gal80, hs-FLP, w*; ppk-Gal4, UAS-mCD8GFP, SOP-flp / UAS-AMPK*.

Figure 2: (A) *w*; ; ppk-Gal4, UAS-mCD8GFP / ppk-Gal4, UAS-mCD8GFP*. **(B) Ctrl RNAi:** *w*; ppk-Gal4, UAS-mCD8GFP, UAS-Dcr2 / ppk-Gal4, UAS-mCD8GFP, UAS-Dcr2;* UAS-Control RNAi / UAS-Control RNAi. ***cnc* RNAi #1:** *w*; ppk-Gal4, UAS-mCD8GFP, UAS-Dcr2 / ppk-Gal4, UAS-mCD8GFP, UAS-Dcr2; UAS-cnc* RNAi #1 / *UAS-cnc* RNAi #1. ***cnc* RNAi #2:** *w*; UAS-cnc* RNAi #2 / *UAS-cnc* RNAi #2; *ppk-Gal4, UAS-mCD8GFP / ppk-Gal4, UAS-mCD8GFP*. **(C) Ctrl RNAi:** *w*; UAS-Dcr2 / +; ppk-Gal4, UAS-mCD8GFP* / UAS-Control RNAi. ***EcR* RNAi:** *w*; UAS-Dcr2 / +; ppk-Gal4, UAS-mCD8GFP / UAS-EcR* RNAi. ***sox14* RNAi:** *w*; UAS-Dcr2 / +; ppk-Gal4, UAS-mCD8GFP* / *UAS-sox14* RNAi. **(D) O/E Control:** *w*; ppk-Gal4, UAS-mCD8GFP / ppk-Gal4, UAS-mCD8GFP; UAS-Mical^{NT} / UAS-Mical^{NT}*. ***O/E CncC:*** *w*; ppk-Gal4, UAS-mCD8GFP / ppk-Gal4, UAS-mCD8GFP; UAS-CncC / UAS-CncC*. ***O/E Sox14:*** *w*; ppk-Gal4 / +; ppk-Gal4, UAS-mCD8GFP / UAS-Sox14*

Figure 3: (A) Ctrl RNAi: *w*;* UAS-Control RNAi / *gstD1-lacZ*; *ppk-Gal4, UAS-mCD8GFP, UAS-Dcr2 / ppk-Gal4, UAS-mCD8GFP*. ***AMPK* RNAi #1:** *w*; UAS-AMPK* RNAi #1 / *gstD1-lacZ*; *ppk-Gal4, UAS-mCD8GFP, UAS-Dcr2 / ppk-Gal4, UAS-mCD8GFP*. ***AMPK* RNAi #2:** *w*; ppk-Gal4, UAS-mCD8GFP, UAS-Dcr2 / gstD1-lacZ; UAS-AMPK* RNAi #2 / *ppk-Gal4, UAS-mCD8GFP*. **(B-C) Ctrl RNAi:** *w*;* UAS-Control RNAi / UAS-Control RNAi; *ppk-Gal4, UAS-mCD8GFP, UAS-Dcr2 / ppk-Gal4, UAS-mCD8GFP,*

Development • Supplementary information

UAS-Dcr2. ***AMPK* RNAi #1:** *w*; UAS-AMPK* RNAi #1 / *UAS-AMPK* RNAi #1; *ppk-Gal4, UAS-mCD8GFP, UAS-Dcr2 / ppk-Gal4, UAS-mCD8GFP, UAS-Dcr2*. ***AMPK* RNAi #2:** *w*; ppk-Gal4, UAS-mCD8GFP, UAS-Dcr2 / ppk-Gal4, UAS-mCD8GFP, UAS-Dcr2; UAS-AMPK* RNAi #2 / *UAS-AMPK* RNAi #2. **(D-E) O/E Control:** *w*; UAS-Dcr2 / UAS-Dcr2; ppk-Gal4, UAS-mCD8GFP / ppk-Gal4, UAS-mCD8GFP*. ***O/E AMPK*:** *w*; UAS-AMPK / UAS-AMPK; ppk-Gal4, UAS-mCD8GFP / ppk-Gal4, UAS-mCD8GFP*. ***O/E AMPK^{CA}*:** *w*; UAS-AMPK^{CA} / UAS-AMPK^{CA}; ppk-Gal4, UAS-mCD8GFP / ppk-Gal4, UAS-mCD8GFP*.

Figure 4: (A) *AMPK* RNAi #1 + O/E Control: *w*; UAS-AMPK* RNAi #1 / *ppk-Gal4, gstD1-lacZ*; *ppk-Gal4, UAS-mCD8GFP, UAS-Dcr2 / UAS-Mical^{NT}*. ***AMPK* RNAi #1 + *O/E CncC*:** *w*; UAS-AMPK* RNAi #1 / *ppk-Gal4, gstD1-lacZ*; *ppk-Gal4, UAS-mCD8GFP, UAS-Dcr2 / UAS-CncC*. ***AMPK* RNAi #2 + O/E Control:** *w*; ppk-Gal4, UAS-mCD8GFP, UAS-Dcr2 / ppk-Gal4, gstD1-lacZ*; *UAS-AMPK* RNAi #2 / *UAS-Mical^{NT}*. ***AMPK* RNAi #2 + *O/E CncC*:** *w*; ppk-Gal4, UAS-mCD8GFP, UAS-Dcr2 / ppk-Gal4, gstD1-lacZ*; *UAS-AMPK* RNAi #2 / *UAS-CncC*. **(B-D) *AMPK* RNAi #1 + O/E Control:** *w*; UAS-AMPK* RNAi #1 / *ppk-Gal4, UAS-mCD8GFP*; *ppk-Gal4, UAS-mCD8GFP, UAS-Dcr2 / UAS-Mical^{NT}*. ***AMPK* RNAi #1 + *O/E CncC*:** *w*; UAS-AMPK* RNAi #1 / *ppk-Gal4, UAS-mCD8GFP*; *ppk-Gal4, UAS-mCD8GFP, UAS-Dcr2 / UAS-CncC*. ***AMPK* RNAi #2 + O/E Control:** *w*; ppk-Gal4, UAS-mCD8GFP, UAS-Dcr2 / ppk-Gal4, UAS-mCD8GFP*; *UAS-AMPK* RNAi #2 / *UAS-Mical^{NT}*. ***AMPK* RNAi #2 + *O/E CncC*:** *w*; ppk-Gal4, UAS-mCD8GFP, UAS-Dcr2 / ppk-Gal4, UAS-mCD8GFP*; *UAS-AMPK* RNAi #2 / *UAS-CncC*.

Figure 5: (A) O/E Control: *w*; UAS-Dcr2 / gstD1-lacZ; ppk-Gal4, UAS-mCD8GFP / ppk-Gal4, UAS-mCD8GFP*. ***O/E InR^{CA}*:** *w*; UAS-InR^{CA} / gstD1-lacZ; ppk-Gal4, UAS-mCD8GFP / ppk-Gal4, UAS-mCD8GFP*. ***O/E Akt:*** *w*; UAS-Akt / gstD1-lacZ; ppk-Gal4, UAS-mCD8GFP / ppk-Gal4, UAS-mCD8GFP*. ***O/E S6K^{CA}:*** *w*; UAS-S6K^{CA} / gstD1-lacZ; ppk-Gal4, UAS-mCD8GFP / ppk-Gal4, UAS-mCD8GFP*. **(B-C) O/E Control:** *w*; UAS-Dcr2 / UAS-Dcr2; ppk-Gal4, UAS-mCD8GFP / ppk-Gal4, UAS-mCD8GFP*. ***O/E InR^{CA}*:** *w*; UAS-InR^{CA} / UAS- InR^{CA}; ppk-Gal4, UAS-mCD8GFP / ppk-Gal4, UAS-mCD8GFP*. ***O/E Akt:*** *w*; UAS-Akt / UAS-Akt; ppk-Gal4, UAS-mCD8GFP / ppk-Gal4, UAS-mCD8GFP*. ***O/E Tor:*** *w*; ppk-Gal4, UAS-mCD8GFP / ppk-Gal4, UAS-mCD8GFP; UAS-Tor / UAS-Tor*. **(D) *O/E InR^{CA}* + O/E Control:**

Development • Supplementary information

w; UAS-InR^{CA} / ppk-Gal4, gstD1-lacZ; ppk-Gal4, UAS-mCD8GFP / UAS-Mical^{NT}*. ***O/E InR^{CA}* + *O/E CncC*:** *w*; UAS-InR^{CA} / ppk-Gal4, gstD1-lacZ; ppk-Gal4, UAS-mCD8GFP / UAS-CncC*. ***O/E S6K^{CA}* + O/E Control:** *w*; UAS-S6K^{CA} / ppk-Gal4, gstD1-lacZ; ppk-Gal4, UAS-mCD8GFP / UAS-Mical^{NT}*. ***O/E* S6K^{CA} + *O/E CncC*:** *w*; UAS-S6K^{CA} / ppk-Gal4, gstD1-lacZ; ppk-Gal4, UAS-mCD8GFP / UAS-CncC*. **(E)** ***O/E InR^{CA}* + O/E Control:** *w*; UAS-InR^{CA} / ppk-Gal4, UAS-mCD8GFP; ppk-Gal4, UAS-mCD8GFP / UAS-Mical^{NT}*. ***O/E InR^{CA}* + *O/E CncC*:** *w*; UAS-InR^{CA} / ppk-Gal4, UAS-mCD8GFP; ppk-Gal4, UAS-mCD8GFP / UAS-CncC*. ***O/E S6K^{CA}* + O/E Control:** *w*; UAS-S6K^{CA} / ppk-Gal4, UAS-mCD8GFP; ppk-Gal4, UAS-mCD8GFP / UAS-Mical^{NT}*. ***O/E* S6K^{CA} + *O/E CncC*:** *w*; UAS- S6K^{CA} / ppk-Gal4, UAS-mCD8GFP; ppk-Gal4, UAS-mCD8GFP / UAS-CncC*.

Figure 6: (A) *w*; UAS-AMPK* RNAi #1 / *UAS-Dcr2*; *ppk-Gal4, UAS-mCD8GFP, UAS-Dcr2 / ppk-Gal4, UAS-mCD8GFP*. **(B)** *w*; UAS-AMPK* RNAi #1 / *UAS-InR^{DN}*; *ppk-Gal4, UAS-mCD8GFP, UAS-Dcr2 / ppk-Gal4, UAS-mCD8GFP*. **(C)** *w*; UAS-AMPK* RNAi #1 / *UAS-PI3K^{DN}*; *ppk-Gal4, UAS-mCD8GFP, UAS-Dcr2 / ppk-Gal4, UAS-mCD8GFP*. **(D)** *w*; UAS-AMPK* RNAi #1 / *ppk-Gal4, UAS-mCD8GFP, UAS-Dcr2*; *ppk-Gal4, UAS-mCD8GFP, UAS-Dcr2 / UAS-Control* RNAi. **(E)** *w*; UAS-AMPK* RNAi #1 / *ppk-Gal4, UAS-mCD8GFP, UAS-Dcr2*; *ppk-Gal4, UAS-mCD8GFP, UAS-Dcr2 / UAS-akt* RNAi. **(F)** *w*; UAS-AMPK* RNAi #1 / +; *ppk-Gal4, UAS-mCD8GFP, UAS-Dcr2 / UAS-Mical^{NT}*. **(G)** *w*; UAS-AMPK* RNAi #1 / *UAS-TSC1,TSC2*; *ppk-Gal4, UAS-mCD8GFP, UAS-Dcr2 / +*. **(H)** *w*; UAS-AMPK* RNAi #1 / *UAS-Tor^{TED}*; *ppk-Gal4, UAS-mCD8GFP, UAS-Dcr2 / +*. **(I)** *w*; UAS-AMPK* RNAi #1 / *UAS- S6K^{DN}*; *ppk-Gal4, UAS-mCD8GFP, UAS-Dcr2 / +*. **(J)** *w*; UAS-AMPK* RNAi #1 / +; *ppk-Gal4, UAS-mCD8GFP, UAS-Dcr2 / UAS-4E-BP(AA)*.

Figure 7: (A) ***O/E Sox14* + Ctrl RNAi:** *w*; ppk-Gal4, gstD1-lacZ / UAS*-Control RNAi *; UAS-Sox14 / ppk-Gal4, UAS-mCD8GFP, UAS-Dcr2*. ***O/E Sox14* + *AMPK* RNAi #1:** *w*; ppk-Gal4, gstD1-lacZ / UAS-AMPK* RNAi #1*; UAS-Sox14 / ppk-Gal4, UAS-mCD8GFP, UAS-Dcr2*. ***O/E Sox14* + O/E Control:** *w*; ppk-Gal4, gstD1-lacZ / UAS-Dcr2; UAS-Sox14 / ppk-Gal4, UAS-mCD8GFP*. ***O/E Sox14* + *O/E InR^{CA}*:** *w*; ppk-Gal4, gstD1-lacZ / UAS-InR^{CA}; UAS-Sox14 / ppk-Gal4, UAS-mCD8GFP*. ***O/E Sox14* + *O/E Akt*:** *w*; ppk-Gal4, gstD1-lacZ / UAS-Akt; UAS-Sox14 / ppk-Gal4, UAS-mCD8GFP*. **(B-C)** ***O/E Sox14* + Ctrl**

Development • Supplementary information

RNAi: *w*; ppk-Gal4, UAS-mCD8GFP / UAS-*Control RNAi*; UAS-Sox14 / ppk-Gal4, UAS-mCD8GFP, UAS-Dcr2.* ***O/E Sox14 + AMPK*** **RNAi #1:** *w*; ppk-Gal4, UAS-mCD8GFP / UAS-AMPK* RNAi #1, *UAS-Dcr2; UAS-Sox14 / ppk-Gal4, UAS-mCD8GFP, UAS-Dcr2.* ***O/E Sox14*** **+ O/E Control:** *w*; ppk-Gal4, UAS-mCD8GFP / UAS-Dcr2; UAS-Sox14 / ppk-Gal4, UAS-mCD8GFP.* ***O/E Sox14 + O/E InR^{CA}:*** *w*; ppk-Gal4, UAS-mCD8GFP / UAS-InR^{CA}; UAS-Sox14 / ppk-Gal4, UAS-mCD8GFP.* ***O/E Sox14 + O/E Akt:*** *w*; ppk-Gal4, UAS-mCD8GFP / UAS-Akt; UAS-Sox14 / ppk-Gal4, UAS-mCD8GFP.*

Figure S1: (B) O/E Control: *w*; ppk-Gal4 / +; UAS-Mical^{NT} / ppk-Gal4, UAS-mCD8GFP.* ***O/E AMPK:*** *w*; UAS-AMPK / ppk-Gal4; + / ppk-Gal4, UAS-mCD8GFP.* ***O/E AMPK^{CA}:*** *w*; UAS-AMPK^{CA} / ppk-Gal4; + / ppk-Gal4, UAS-mCD8GFP.*

Figure S2: (A-D) WT: *w*; ; ppk-Gal4, UAS-mCD8GFP / ppk-Gal4, UAS-mCD8GFP.* ***AMPK*** **RNAi #1:** *w*; UAS-AMPK* RNAi #1 / *UAS-AMPK* RNAi #1; *ppk-Gal4, UAS-mCD8GFP, UAS-Dcr2 / ppk-Gal4, UAS-mCD8GFP, UAS-Dcr2.* ***O/E AMPK^{KR}:*** *w*; ppk-Gal4, UAS-mCD8GFP / ppk-Gal4, UAS-mCD8GFP; UAS-AMPK^{KR} / UAS-AMPK^{KR}.*

Figure S3: (B) *w*; ppk-Gal4, UAS-mCD8GFP / ppk-Gal4, UAS-mCD8GFP; mical1-lacZ / mical1-lacZ.* **(C)** *w*; ppk-Gal4 / ppk-Gal4; ppk-Gal4, UAS-mCD8GFP / ppk-Gal4, UAS-mCD8GFP.* **(D) Ctrl RNAi:** *w*; ppk-Gal4, UAS-mCD8GFP, UAS-Dcr2 / +; UAS-Control* RNAi */ mical1-lacZ.* ***EcR*** **RNAi:** *w*; ppk-Gal4, UAS-mCD8GFP, UAS-Dcr2 / +; UAS-EcR* RNAi */ mical1-lacZ.* ***sox14*** **RNAi:** *w*; ppk-Gal4, UAS-mCD8GFP, UAS-Dcr2 / +; UAS-sox14* RNAi */ mical1-lacZ.* **(E) Ctrl RNAi:** *w*; ppk-Gal4, UAS-mCD8GFP, UAS-Dcr2 / +; UAS-Control* RNAi */ mical1-lacZ.* ***AMPK*** **RNAi #1:** *w*; UAS-AMPK* RNAi #1 */ +; ppk-Gal4, UAS-mCD8GFP, UAS-Dcr2 / mical1-lacZ.* ***O/E AMPK^{KR}:*** *w*; ppk-Gal4, UAS-mCD8GFP / +; UAS-AMPK^{KR} / mical1-lacZ.*

Figure S4: (A) Ctrl RNAi: *w*; UAS-Dcr2 / +; ppk-Gal4, UAS-mCD8GFP / UAS-Control* RNAi.* ***rpn7*** **RNAi #1:** *w*; UAS-Dcr2 / +; ppk-Gal4, UAS-mCD8GFP / UAS-rpn7* RNAi #1.* ***rpn7*** **RNAi #2:** *w*; UAS-Dcr2 / UAS-rpn7* RNAi #2*; ppk-Gal4, UAS-mCD8GFP / +.* ***mical*** **RNAi:** *w*; ppk-Gal4, UAS-mCD8GFP, UAS-Dcr2 / ppk-Gal4, UAS-mCD8GFP, UAS-Dcr2; UAS-mical* RNAi / *UAS-mical* RNAi.* **(B) Ctrl RNAi:** *w*; UAS-Dcr2 / +; ppk-Gal4, UAS-mCD8GFP / UAS-Control* RNAi.* ***rpn7*** **RNAi #1:** *w*; UAS-Dcr2 / +;*

Development • Supplementary information

ppk-Gal4, UAS-mCD8GFP / UAS-rpn7 RNAi #1. ***rpn7* RNAi #2:** *w*; UAS-Dcr2 / UAS-rpn7* RNAi #2*; ppk-Gal4, UAS-mCD8GFP / +*. **(C) O/E Control:** *w*; ppk-Gal4, UAS-mCD8GFP / ppk-Gal4, UAS-mCD8GFP; UAS-Mical^{NT} / UAS-Mical^{NT}*. ***O/E CncC:*** *w*; ppk-Gal4, UAS-mCD8GFP / ppk-Gal4, UAS-mCD8GFP; UAS-CncC / UAS-CncC*. ***O/E Sox14:*** *w*; ppk-Gal4 / +; ppk-Gal4, UAS-mCD8GFP / UAS-Sox14*.

Figure S5: (A) Ctrl RNAi: *w*;* UAS-Control RNAi / UAS-Control RNAi; *ppk-Gal4, UAS-mCD8GFP, UAS-Dcr2 / ppk-Gal4, UAS-mCD8GFP, UAS-Dcr2*. ***AMPK* RNAi #1:** *w*; UAS-AMPK* RNAi #1 / *UAS-AMPK* RNAi #1; *ppk-Gal4, UAS-mCD8GFP, UAS-Dcr2 / ppk-Gal4, UAS-mCD8GFP, UAS-Dcr2*. **O/E Control***: w*; ppk-Gal4, UAS-mCD8GFP / ppk-Gal4, UAS-mCD8GFP; UAS-Mical^{NT} / UAS- Mical^{NT}*. ***O/E AMPK^{KR}****: w*; ppk-Gal4, UAS-mCD8GFP / ppk-Gal4, UAS-mCD8GFP; UAS-AMPK^{KR} / UAS-AMPK^{KR}*. **(B)Ctrl RNAi:** *w*;* UAS-Control RNAi / UAS-Control RNAi; *ppk-Gal4, UAS-mCD8GFP, UAS-Dcr2 / ppk-Gal4, UAS-mCD8GFP, UAS-Dcr2*. ***AMPK* RNAi #1:** *w*; UAS-AMPK* RNAi #1 / *UAS-AMPK* RNAi #1; *ppk-Gal4, UAS-mCD8GFP, UAS-Dcr2 / ppk-Gal4, UAS-mCD8GFP, UAS-Dcr2*. **(C) O/E Control:** *w*; Gal4$^{4-77}$, UAS-EB1-GFP / +; + / UAS-Mical^{NT}*. ***O/E AMPK^{KR}****: w*; Gal4$^{4-77}$, UAS-EB1-GFP / +; + / UAS-AMPK^{KR}*.

Figure S6: (A) *O/E Rab5^{DN}* + O/E Control: *w*; ppk-Gal4, UAS-mCD8GFP / ppk-Gal4, UAS-Rab5^{DN} ; ppk-Gal4, UAS-mCD8GFP / UAS-Mical^{NT}*. ***O/E Rab5^{DN}* + *O/E CncC*:** *w*; ppk-Gal4, UAS-mCD8GFP / ppk-Gal4, UAS-Rab5^{DN} ; ppk-Gal4, UAS-mCD8GFP / UAS-CncC*. **(B) *cnc* RNAi #1 + Ctrl RNAi:** *w*; ppk-Gal4, UAS-mCD8GFP, UAS-Dcr2* / UAS-Control RNAi; *UAS-cnc* RNAi #1*/ ppk-Gal4, UAS-mCD8GFP, UAS-Dcr2*. ***AMPK* RNAi #1 + Ctrl RNAi:** *w*; ppk-Gal4, UAS-mCD8GFP, UAS-Dcr2 / UAS-AMPK* RNAi #1; *UAS*-Control RNAi */ ppk-Gal4, UAS-mCD8GFP, UAS-Dcr2*. ***AMPK* RNAi #1 + *cnc* RNAi:** *w*; ppk-Gal4, UAS-mCD8GFP, UAS-Dcr2 / UAS-AMPK* RNAi #1; *UAS-cnc* RNAi #1 */ ppk-Gal4, UAS-mCD8GFP, UAS-Dcr2*. **(C) *AMPK* RNAi #1 + O/E Control:** *w*; UAS-AMPK* RNAi #1 / *ppk-Gal4, UAS-mCD8GFP*; *ppk-Gal4, UAS-mCD8GFP, UAS-Dcr2 / UAS-Mical^{NT}*. ***AMPK* RNAi #1 + *O/E CncC*:** *w*; UAS-AMPK* RNAi #1 / *ppk-Gal4, UAS-mCD8GFP*; *ppk-Gal4, UAS-mCD8GFP, UAS-Dcr2 / UAS-CncC*. **(D) AMPK RNAi #1 + O/E Control; Control:** *w*; UAS-AMPK* RNAi #1 / *UAS-Mical^{NT}*; *ppk-*

Development • Supplementary information

Gal4, UAS-mCD8GFP, UAS-Dcr2 / UAS-Mical^{NT}. **AMPK RNAi #1 + O/E Control; *Mical*:** *w*; UAS-AMPK* RNAi #1 / *UAS-Mical*^{NT}; *ppk-Gal4, UAS-mCD8GFP, UAS-Dcr2 / UAS-Mical*. ***AMPK* RNAi #1 + O/E Control; *CncC* :** *w*; UAS-AMPK* RNAi #1 / *UAS-Mical*^{NT}; *ppk-Gal4, UAS-mCD8GFP, UAS-Dcr2 / UAS-CncC*. ***AMPK* RNAi #1 + *O/E CncC, Mical*:** *w*; UAS-AMPK* RNAi #1 / +; *ppk-Gal4, UAS-mCD8GFP, UAS-Dcr2 / UAS-CncC, UAS-Mical*. **(E-F) *cnc* RNAi #1 + O/E Control:** *w*; ppk-Gal4, UAS-mCD8GFP, UAS-Dcr2* / UAS-Dcr2; *UAS-cnc* RNAi #1/ *ppk-Gal4, UAS-mCD8GFP*. ***cnc* RNAi #1 + *O/E AMPK*:** *w*; ppk-Gal4, UAS-mCD8GFP, UAS-Dcr2* / *UAS-AMPK*; *UAS-cnc* RNAi #1/ *ppk-Gal4, UAS-mCD8GFP*. ***cnc* RNAi #1 + *O/E AMPK*^{CA}:** *w*; ppk-Gal4, UAS-mCD8GFP, UAS-Dcr2* / *UAS-AMPK*^{CA}; *UAS-cnc* RNAi #1/ *ppk-Gal4, UAS-mCD8GFP*.

Figure S7: (A) O/E Control: *w*; UAS-Dcr2 / UAS-Dcr2; ppk-Gal4, UAS-mCD8GFP / ppk-Gal4, UAS-mCD8GFP*. ***O/E InR*^{CA}:** *w*; UAS-InR*^{CA} */ UAS-InR*^{CA}*; ppk-Gal4, UAS-mCD8GFP / ppk-Gal4, UAS-mCD8GFP*. ***O/E Akt:*** *w*; UAS-Akt / UAS-Akt; ppk-Gal4, UAS-mCD8GFP / ppk-Gal4, UAS-mCD8GFP*. ***O/E TOR:*** *w*; ppk-Gal4, UAS-mCD8GFP / ppk-Gal4, UAS-mCD8GFP; UAS-Tor / UAS-TOR*. **(B) O/E Control:** *w*; UAS-Dcr2* / *gstD1-lacZ*; *ppk-Gal4, UAS-mCD8GFP* / *ppk-Gal4, UAS-mCD8GFP*. ***O/E InR*^{DN}:** *w*; UAS-InR*^{DN} / *gstD1-lacZ*; *ppk-Gal4, UAS-mCD8GFP* / *ppk-Gal4, UAS-mCD8GFP*. ***O/E PI3K*^{DN}:** *w*; UAS-PI3K*^{DN} / *gstD1-lacZ*; *ppk-Gal4, UAS-mCD8GFP* / *ppk-Gal4, UAS-mCD8GFP*. ***O/E S6K*^{DN}:** *w*; UAS-S6K*^{DN} / *gstD1-lacZ*; *ppk-Gal4, UAS-mCD8GFP* / *ppk-Gal4, UAS-mCD8GFP*. **Ctrl RNAi**: *w*; ppk-Gal4, UAS-mCD8GFP, UAS-Dcr2* / *gstD1-lacZ*; *UAS-control* RNAi / *ppk-Gal4, UAS-mCD8GFP*. ***akt* RNAi:** *w*; ppk-Gal4, UAS-mCD8GFP, UAS-Dcr2* / *gstD1-lacZ*; *UAS-akt* RNAi / *ppk-Gal4, UAS-mCD8GFP*. **(C) O/E Control:** *w*; UAS-Dcr2* / *UAS-Dcr2*; *ppk-Gal4, UAS-mCD8GFP / ppk-Gal4, UAS-mCD8GFP*. ***O/E InR*^{DN}:** *w*; UAS-InR*^{DN} / *UAS-InR*^{DN}; *ppk-Gal4, UAS-mCD8GFP / ppk-Gal4, UAS-mCD8GFP*. ***O/E PI3K*^{DN}:** *w*; UAS-PI3K*^{DN} / UAS-*PI3K*^{DN}; *ppk-Gal4, UAS-mCD8GFP / ppk-Gal4, UAS-mCD8GFP*. ***O/E S6K*^{DN}:** *w*; UAS-S6K*^{DN} / UAS-*S6K*^{DN}; *ppk-Gal4, UAS-mCD8GFP / ppk-Gal4, UAS-mCD8GFP*. **Ctrl RNAi**: *w*; ppk-Gal4, UAS-mCD8GFP, UAS-Dcr2* / *ppk-Gal4, UAS-mCD8GFP*, UAS-Dcr2; *UAS*-control RNAi / *UAS*-control RNAi. ***akt* RNAi:** *w*; ppk-Gal4, UAS-mCD8GFP, UAS-Dcr2* / *ppk-Gal4, UAS-mCD8GFP*, UAS-Dcr2; *UAS-akt* RNAi / *UAS-akt* RNAi.

Development • Supplementary information

Figure S8: (A-B) *cnc* RNAi #1 + O/E Control: *w*; ppk-Gal4, UAS-mCD8GFP, UAS-Dcr2* / UAS-Dcr2; *UAS-cnc* RNAi #1/ *ppk-Gal4, UAS-mCD8GFP*. ***cnc* RNAi #1 + *O/E PI3K^{DN}*:** *w*; ppk-Gal4, UAS-mCD8GFP, UAS-Dcr2* / *UAS-PI3K^{DN}*; *UAS-cnc* RNAi #1/ *ppk-Gal4, UAS-mCD8GFP*. ***cnc* RNAi #1 + *O/E TOR^{TED}*:** *w*; ppk-Gal4, UAS-mCD8GFP, UAS-Dcr2* / *UAS-TOR^{TED}*; *UAS-cnc* RNAi #1/ *ppk-Gal4, UAS-mCD8GFP*. ***cnc* RNAi #1 + *O/E S6K^{DN}*:** *w*; ppk-Gal4, UAS-mCD8GFP, UAS-Dcr2* / *UAS-S6K^{DN}*; *UAS-cnc* RNAi #1/ *ppk-Gal4, UAS-mCD8GFP*.

Figure S9: (A) O/E Control: *w*; ppk-Gal4, UAS-mCD8GFP / gstD1-lacZ; UAS-Mical^{NT} / ppk-Gal4, UAS-mCD8GFP*. ***O/E Mts^{DN}:*** *w*; ppk-Gal4, UAS-mCD8GFP / gstD1-lacZ; UAS-Mts^{DN} / ppk-Gal4, UAS-mCD8GFP*. **Ctrl RNAi**: *w*; ppk-Gal4, UAS-mCD8GFP, UAS-Dcr2 / gstD1-lacZ;* UAS-control RNAi / *ppk-Gal4, UAS-mCD8GFP*. ***PP2A-29B* RNAi:** *w*; ppk-Gal4, UAS-mCD8GFP, UAS-Dcr2 / gstD1-lacZ; UAS-PP2A-29B* RNAi / *ppk-Gal4, UAS-mCD8GFP*. **(B-C) Ctrl RNAi:** *w*; ppk-Gal4, UAS-mCD8GFP, UAS-Dcr2 / ppk-Gal4, UAS-mCD8GFP, UAS-Dcr2;* UAS-Control RNAi / UAS-Control RNAi. ***mts* RNAi:** *w*; UAS-mts* RNAi / *UAS-Dcr2; ppk-Gal4, UAS-mCD8GFP / +*. ***PP2A-29B* RNAi:** *w*; ppk-Gal4, UAS-mCD8GFP, UAS-Dcr2 / ppk-Gal4, UAS-mCD8GFP, UAS-Dcr2; UAS-PP2A-29B* RNAi / *UAS-PP2A-29B* RNAi. **(D) *O/E Mts^{DN}* + Ctrl RNAi:** *w*; ppk-Gal4, UAS-mCD8GFP / ppk-Gal4, UAS-mCD8GFP, UAS-Dcr2; UAS-Mts^{DN} / UAS*-Control RNAi. ***O/E Mts^{DN}* + *akt* RNAi:** *w*; ppk-Gal4, UAS-mCD8GFP / ppk-Gal4, UAS-mCD8GFP, UAS-Dcr2; UAS-Mts^{DN} / UAS-akt* RNAi. ***O/E Mts^{DN}* + O/E Control:** *w*; ppk-Gal4, UAS-mCD8GFP / ppk-Gal4, UAS-mCD8GFP; UAS-Mts^{DN} / UAS-Mical^{NT}*. ***O/E Mts^{DN}* + *O/E Tor^{TED}*:** *w*; ppk-Gal4, UAS-mCD8GFP / UAS-Tor^{TED}; UAS-Mts^{DN} / ppk-Gal4, UAS-mCD8GFP* .

Figure S10 (B) *AMPK* RNAi #1 + O/E Control: *w*; UAS-AMPK* RNAi #1 / *UAS-Dcr2; ppk-Gal4, UAS-mCD8GFP, UAS-Dcr2 / ppk-Gal4, UAS-mCD8GFP*. ***AMPK* RNAi #1 + *O/E InR^{DN}*:** *w*; UAS-AMPK* RNAi #1 / *UAS-InR^{DN}*; *ppk-Gal4, UAS-mCD8GFP, UAS-Dcr2 / ppk-Gal4, UAS-mCD8GFP*. ***AMPK* RNAi #1 + *O/E PI3K^{DN}*:** *w*; UAS-AMPK* RNAi #1 / *UAS-PI3K^{DN}*; *ppk-Gal4, UAS-mCD8GFP, UAS-Dcr2 / ppk-Gal4, UAS-mCD8GFP*. ***AMPK* RNAi #1 + *O/E TSC1/2*:** *w*; UAS-AMPK* RNAi #1 / *UAS-TSC1/2; ppk-Gal4, UAS-mCD8GFP, UAS-Dcr2 / +*. ***AMPK* RNAi #1 + *O/E TOR^{TED}*:** *w*; UAS-AMPK* RNAi #1 / *UAS-TOR^{TED}; ppk-Gal4, UAS-mCD8GFP, UAS-Dcr2 / +*. ***AMPK* RNAi #1 + *O/E S6K^{DN}*:** *w*; UAS-AMPK*

Development • Supplementary information

RNAi #1 / *UAS- S6K^{DN}; ppk-Gal4, UAS-mCD8GFP, UAS-Dcr2 / +*. **(C) AMPK RNAi #1 + O/E Control; Control:** *w*; UAS-AMPK* RNAi #1 / *UAS-Mical^{NT}*; *ppk-Gal4, UAS-mCD8GFP, UAS-Dcr2 / UAS-Mical^{NT}*. ***AMPK* RNAi #1 + O/E Control; *Mical*:** *w*; UAS-AMPK* RNAi #1 / *UAS-Mical^{NT}*; *ppk-Gal4, UAS-mCD8GFP, UAS-Dcr2 / UAS-Mical*. ***AMPK* RNAi #1 + O/E *InR^{DN}*; Control:** *w*; UAS-AMPK* RNAi #1 / *UAS-InR^{DN}*; *ppk-Gal4, UAS-mCD8GFP, UAS-Dcr2 / UAS-Mical^{NT}*. ***AMPK* RNAi #1 + *O/E InR^{DN}*; *Mical*:** *w*; UAS-AMPK* RNAi #1 / *UAS-InR^{DN}*; *ppk-Gal4, UAS-mCD8GFP, UAS-Dcr2 / UAS-Mical*. **(D) *O/E InR^{CA}* + O/E Control:** *w*; UAS-InR^{CA} / UAS-Dcr2; ppk-Gal4, UAS-mCD8GFP / ppk-Gal4, UAS-mCD8GFP*. ***O/E InR^{CA}* + *O/E AMPK^{CA}*:** *w*; UAS-InR^{CA} / UAS- AMPK^{CA}; ppk-Gal4, UAS-mCD8GFP / ppk-Gal4, UAS-mCD8GFP*. ***O/E TOR* + O/E Control:** *w*; ppk-Gal4, UAS-mCD8GFP / UAS-Dcr2; ppk-Gal4, UAS-mCD8GFP / UAS-TOR*. ***O/E TOR* + *O/E AMPK^{CA}*:** *w*; ppk-Gal4, UAS-mCD8GFP / UAS-AMPK^{CA}; ppk-Gal4, UAS-mCD8GFP / UAS-TOR*.

Table S1. Source data for all the figures

Click here to download Table S1

Development • Supplementary information